3.6.2 CCSEM Analysis

In order to gain an understanding of the changes in size and association that occur in the inorganic matter in low-rank coal during combustion, quantitative information about the types and size distributions of the discrete mineral grains must be obtained. A number of different avenues for obtaining some of this information exists, although each has certain weaknesses. Some methods commonly used are x-ray diffraction, infrared spectroscopy, and normative analysis (12). One problem with the x-ray diffraction and infrared spectroscopy techniques is that the mineral matter needs to be separated from the coal. The most common separation technique is low-temperature ashing (LTA). Unfortunately, the LTA process causes the formation of artifact minerals from the organically associated elements in the coal (12). This is especially a problem when ashing low-rank coals because of the large quantity of organically associated elements that occur in low-rank coals. The organically associated elements in low-rank coals also create large errors when normative calculations are used to quantify coal mineral matter. In addition, none of these techniques gives any information about the size distributions of the mineral matter in the coal.

The ideal quantitative mineralogy technique would not require separation of the minerals from the coal, would not be affected by size or shape of the minerals, would be relatively routine, and would give information about the size distribution of the minerals. Computer-controlled scanning electron microscopy (CCSEM) in conjunction with energy-dispersive x-ray analysis comes closest to meeting these criteria (13). The samples were prepared for CCSEM analysis by embedding them in Beuhler Epo-Kwik epoxy in a ratio of 10 parts epoxy to 1 part sample (by weight). The low sample-to-epoxy ratio was employed to reduce the interference in the x-ray signal from the nearby particles. The sample and epoxy were weighed into 2-mL vials, shaken, and stirred with a toothpick. To prevent sedimentation and orienting of the particles during polymerization of the epoxy, the vials were rotated about the long axis of the vial at a rate of approximately 30 rpm until the epoxy set. The vials were then cut in half with a low-deformation diamond saw along a plane perpendicular to the rotation axis. The face of one of the halves was polished with a graded series of diamond pastes to prepare the sample for CCSEM analysis. The finest diamond paste employed was 1/4 μm. Finally, the samples were coated with an approximately 200 angstrom thick layer of carbon to reduce charging during analysis. Each sample was then analyzed with the CCSEM techniques described in section 2.2.

During analysis, the data was continually dumped from the Tracor 5500 to a BASIC file in a personal computer. The data was later reduced using a Fortran program on a MicroVax II minicomputer.

Because the mineral grain size distribution spanned two orders of magnitude, two magnifications were used in the CCSEM analysis. A magnification of 50x was used for particles in the 10- to 100-μm diameter range, and a magnification of 240x was used for particles with diameters of 1 to 10 microns. Either 1000 particles or 10 frames (whichever came first) were analyzed at each magnification. The frames were oriented along diameters across the polished pellet surface. Each frame was adjacent to the previous frame unless

a bubble was evident within the frame, in which case a frame was chosen further along the diameter to exclude the bubble from the frame. Approximately four hours of SEM time per sample is required using this procedure.

Particles smaller than 1 μm were not analyzed because they have small volumes compared to the x-ray excitation volume within the coal-epoxy pellet (14). Figure 23 illustrates the relationship between the electron beam at the surface of the polished cross section of a char particle and the x-ray emission volume within the particle. Note that size considerations prevent the figure from being drawn to scale (if the figure were made to the same scale as the diameter of the electron beam, the diameter of the x-ray emission volume in the figure would have to be approximately 5 feet).

Because the x-ray emission volume within the sample is large compared to the size and distance between ash particles in the 1-μm and smaller size range, x-rays may be emitted from particles adjacent to the particle of interest. This interference can make it impossible to determine the composition of the particle of interest and creates error in the particulate quantification data.

One method of circumventing this problem is to increase the epoxy-to-char/ash ratio in the pellet in order to spread the particles out to reduce the probability that they will become juxtaposed. However, when the sample contains coal or char, increasing the epoxy-to-sample ratio does not eliminate the particle juxtaposition problem because ash particles are often adjacent to each other in the coal or char. Therefore, the composition of particles with diameters less than one micron were determined by TEM-STEM EDS analysis.

3.6.3 TEM Analysis

To reduce the juxtaposition problem when analyzing small particles, particles with a diameter less than 1 μm were analyzed in 0.1- to 0.2-μm thick ultrathin sections of the epoxy-char/ash pellets using a TEM-STEM system. By limiting the sample thickness to only 0.1 to 0.2 μm, the diameter of the x-ray emission volume is limited to between 0.1 and 0.2 μm, and the depth is limited to the thickness of the ultrathin section. Sectioning therefore decreases the problems associated with x-ray emission by particles near the particle of interest. The TEM-STEM system is a Phillips EM420 with an 860 Series II x-ray analyzer.

The ultrathin sections were prepared by first making a sample and resin block similar to that prepared for the analysis of larger particles by CCSEM. However, the method of preparation was slightly different. Instead of using Epo-Kwik epoxy, LR White resin produced by the London Resin Company, Ltd. was used because of its lower viscosity and superior sectioning properties. The preparation procedure involved weighing 0.3 grams of LR White into a large BEEM capsule purchased from Ted Pella Inc. An approximately 0.12-gram sample was added, and the capsule was filled with an additional 0.4 grams of LR White. The lid of the capsule was closed, and the capsule was shaken. The capsule was then placed in a vial clamped to a slowly rotating wheel to keep the sample in suspension in the resin. The capsule was kept rotating for

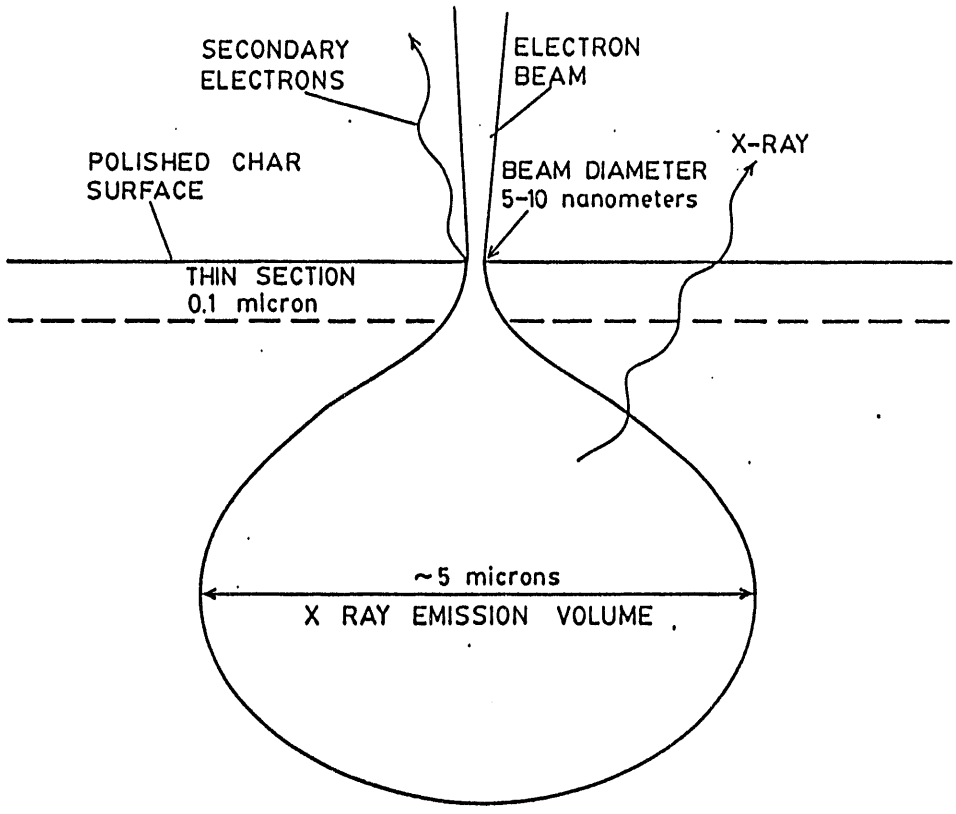

Figure 23. The relationship between the CCSEM electron beam and the x-ray emission volume in a char sample (not to scale).

approximately 1/2 hour to allow the resin to fully penetrate the sample particles. After 1/2 hour, the vial was removed from the wheel, and the BEEM capsule was opened. A toothpick wetted with a polymerization accelerator was used to stir the resin and sample mixture, then the capsule was closed and returned to the vial, and the vial was rotated until polymerization of the resin was complete.

After polymerization, the block face was trimmed with a razor blade to a trapezoidal shape measuring approximately 0.5 millimeters at the base, 0.7 millimeters tall, and 0.3 millimeters at the top. The block was then mounted in an ultramicrotome and sectioned with a glass microtome knife to flatten the face. After the face was flattened, the glass knife was replaced with a diamond knife. The angle between the diamond and the direction of movement of the block in the microtome was maintained at 5°. The velocity of the block past the diamond during sectioning is usually adjusted to between 0.4 and 0.8 millimeters/second.

As sections are cut by the diamond, they float away from the diamond onto the surface of a pool of ethylene glycol held in the "boat" behind the diamond. The level of the ethylene glycol in the boat is maintained at the lowest level possible that will still allow the edge of the knife to be

wetted. Although water is a more preferable boat fluid because it has a lower viscosity, higher surface tension, and does not wet the face of the block as ethylene glycol does, water does dissolve some of the inorganic phases in the sections more readily than ethylene glycol.

3.7 Experimental Measurements

3.7.1 Coal Selection

Two subbituminous coals were used in the present study. One was from the Eagle Butte mine, Wyoming, and the other was from the Robinson Seam, Sarpy Creek mine, Montana. They were chosen for several reasons. One reason is that a barrel of each coal was available from lots on which extensive DOE-funded combustion work was being performed at other institutions, therefore allowing comparisons to be made between the data produced in the present study and the data available from the other studies. Each sample was provided already pulverized to a standard utility grind. The Eagle Butte was provided by Foster Wheeler Development Corporation from a blended lot being used in a DOE-funded (Contract Number DE-AC22-86PC90751) consortium effort administered by Physical Sciences Incorporated (PSI). The consortium is involved in research into the transformation of inorganic coal constituents in combustion systems. Eagle Butte coal was chosen for study by the consortium because it is rich in calcium, which enables examination of the transformation of calcium species during combustion.

The Robinson Seam sample was provided by the University of North Dakota Energy and Environmental Research Center (UNDEERC) in 12 five-gallon bags that were riffled from a larger lot which is being used in drop-tube furnace combustion tests along with Eagle Butte coal from the same lot as the coal used in the present study.

Proximate, ultimate, Btu, and sulfur analyses of each coal are shown in Table 10. The composition of the ASTM ash of the coals is shown in Table 11.

3.7.2 Combustion Test Conditions

3.7.2.1 Reproducibility of Coal-Firing Conditions

All combustion tests were run with a coal feed rate of 200,000 Btu/hr and 20% excess air. Table 12 lists the coal and air feed rates for each coal.

Before beginning any type of sampling, coal firing was maintained until a stable wall temperature above the sampling point was attained. This usually required firing the coal for approximately 10 minutes when sampling near the top of the combustor, but when sampling near the bottom of the combustor it was often necessary to fire on coal for up to 20 minutes before a stable temperature profile was established. For the purposes of this study, a stable wall temperature profile was defined as one that fell within limits established by previous tests lasting at least 30 minutes. In addition, the wall temperature at any point above the sampling point had to vary less than 1°C/minute.

TABLE 10

PROXIMATE, ULTIMATE, BTU, AND SULFUR ANALYSES OF THE TEST COALS (AS-BURNED BASIS, WT%)

	Eagle Butte	Robinson
H_2O	26.0	21.0
Volatile Matter	33.0	29.0
Fixed Carbon	36.0	41.0
Ash	5.4	8.6
C	51.0	53.0
H	6.0	5.4
N	0.6	0.9
S	0.4	0.8
O	36.0	30.0
Calorific Value (Btu/lb)	8580	8850

TABLE 11

ASTM ASH COMPOSITIONS OF THE EAGLE BUTTE AND ROBINSON COALS

Elemental Oxide (wt%)	Eagle Butte	Robinson
Na_2O	2.5	4.7
MgO	7.1	3.5
Al_2O_3	17.0	17.0
SiO_2	32.0	41.0
K_2O	0.3	0.4
CaO	31.0	20.0
TiO_2	1.0	0.7
MnO	0.1	<0.1
Fe_2O_3	8.0	13.0
SO_3	13.0	17.0

TABLE 12

COAL AND AIR FEED RATES

	Robinson	Eagle Butte
Coal (lbs/hr)	23.4	22.4
Primary Air (scfm)	7.6	7.6
Secondary Air (scfm)	34.5	34.7

In practice this meant that the wall temperatures varied from test to test by up to 30-40°C from the median temperatures determined from all tests of a particular coal. A variation of 30-40°C is small, however, compared to the several hundred degree variation in temperatures experienced by inorganic particles in the flame, depending on whether they are inherent within burning coal particles or are extraneous inorganic particles (15).

3.7.2.2 Gas and Particle Temperatures

Figure 24 shows suction pyrometer, wall temperature, and bare thermocouple temperature profiles of the furnace while firing Robinson Seam coal under the conditions listed in Table 12. As can be seen by the observations, the flame is vigorous at the top of the quarl, but it is most vigorous and the gas temperature is highest at the level of the second viewing port in the quarl. At the level of the top port, the flame is quite turbulent, although no recirculation is evident. At the second port and below, the flame is not turbulent, and very little nonaxial flame movement is evident. By the time the gas and particles reach the fourth viewing port, combustion has essentially finished. This is indicated by the facts that almost no glowing particles and only intermittent fingers of flame are seen through this port.

3.7.2.3 Particle Velocity Determinations

The time-dependent position of the extraneous inorganic particles in the combustor is determined with the use of several assumptions. The first is that for inorganic particles less than 35 μm in diameter, the particle velocity under normal flow conditions in the down-fired combustor can be assumed to be the velocity of the gas. This is a valid assumption under normal flow conditions because the terminal velocity of such particles is less than 0.1 ft/s (normal flow conditions is a phrase that is meant to imply flow in the main body of the combustor and not in regions such as the entrance to a sampling device or other regions exhibiting large velocity gradients). Therefore, the task of measuring or calculating gas velocities replaces the more difficult task of directly measuring particle velocities. Unfortunately, measuring the gas velocity in the combustor is made complex by the high temperatures and the presence of ash in the gas. Commercially available pilot tubes or hot-wire anemometers, equipment often used to measure gas velocities in exit stacks (16), are usually not designed for high-temperature operation. Even if they could be designed to handle the high temperatures, experience with other measuring equipment shows that they would be prone to rapid fouling by the ash. Therefore, the gas velocities were calculated rather than directly measured.

As a first approximation in the calculations, it was assumed that the radial velocity profile was that of a plug flow. This meant that the gas velocity at the center of the combustor was approximately equal to the average gas velocity. This assumption was made because Reynolds number calculations, as well as observations of the coal flame, show that turbulent conditions are present at the top of the quarl. Below the quarl, the Reynolds numbers are approximately 1500-1700, within the range of laminar flow. However, the entrance length under normal firing conditions is in the range of 70 to 80 feet (17), so the flow is not well developed anywhere in the combustor. Since

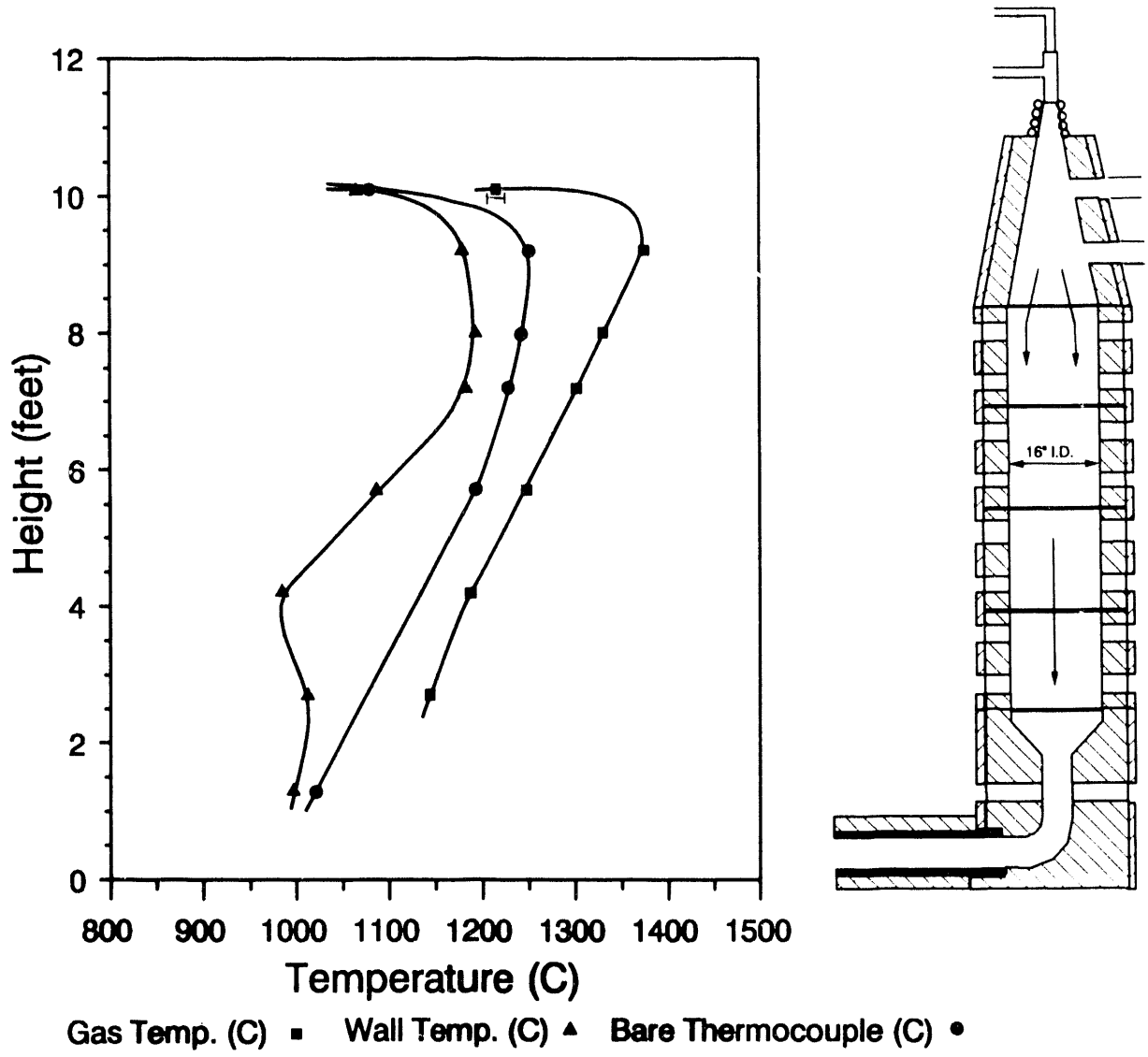

Figure 24. Wall and gas temperature profiles obtained when burning pulverized Robinson Seam coal at 200,000 Btu/hr and 20% excess air.

the lowest sampling point is only eight feet from the turbulent gas flow at the top of the combustor, the assumption of a plug flow velocity profile at the lowest sampling point appeared justified.

Another assumption in the calculations is that any net increase in the standard volume of the combustion gases occurs before the particles reach the top sampling port in the furnace. This is a good assumption because since the complete combustion of carbon creates no net change in moles of gas, and since the increase in moles of gas due to CO formation is negligible, then the greatest increase in gas volume over the volume of the combustion air is due to the evaporation of moisture from the coal. Also, evaporation of moisture is believed to be complete by the time the particles reach the first port

because the gas temperature in the vicinity of the first port is over 1200°C. Other assumptions in the calculations are that the pressure in the combustor does not vary with position, and that the gas is an ideal gas.

Under the assumptions listed above the velocity of the gas in the combustor is given by:

$$V = Q/A \qquad \text{[Eq. 15]}$$

where: V = gas velocity
Q = volumetric flow rate
A = area.

The volumetric flow rate can be calculated from the predicted standard volume of the products of combustion and the absolute temperature of the gas as shown in Equation 16:

$$Q_{actual} = (Q_{standard})T/298\ K \qquad \text{[Eq. 16]}$$

where: Q_{actual} = the actual flow rate in the combustor
$Q_{standard}$ = the flow rate at standard conditions
T = the absolute temperature (K).

To find the total time required for a particle to be carried from the level of the first port (the highest point at which gas and wall temperatures are measured) to another point within the combustion chamber, the gas temperature must be written as a function of position. The simplest way to do this is to use a computer code to fit a polynomial of suitable degree to the absolute temperature versus position data. To reach a correlation coefficient of 0.99, a fifth-degree polynomial was required. It is given in Equation 17:

$$T = 1491 + 354.6X - 260.7 \times 2 + 76.27 \times 3 + -10.08 \times 4 + 0.4915 \times 5 \qquad \text{[Eq. 17]}$$

The cross-sectional area of the combustion chamber varies with height within the quarl, but is constant within the main combustion chamber. The area of the chamber within the quarl and below the midpoint of Port 1 is given by equation 18:

$$Area = \pi(rpl + xtanr)^2 \qquad \text{[Eq. 18]}$$

where: rpl = 1/3 ft = the radius of the combustor chamber at Port 1
r = 10° = the half angle of divergence of the quarl
x = the distance below the middle of the first port.

Below the quarl, the cross-sectional area is 1.40 ft^2.

The velocity of the combustion gas, under the assumptions listed above, can then be calculated by substituting Equations 16, 17, and 18 into Equation 1. By rearranging the equation for the definition of velocity given in Equation 19 and integrating as shown in Equation 20, the time needed for a particle to be carried from the level of Port 1 to a point of interest can be calculated.

$$v\ (x) = dx/dt \qquad \text{[Eq. 19]}$$

$$t + c = (298/Q_{standard})(\&(Area(x))dx/T(x) \qquad \text{[Eq. 20]}$$

Figure 25 shows the time-temperature history of a 20-μm diameter extraneous quartz particle during a 200,000-Btu/hr test of the Robinson coal as it passes from the first port to the tenth (second from the bottom) port in the combustor. The times were calculated numerically from Equation 20.

3.7.2.4 Gas Composition Measurements

The composition of the combustor gas versus height in the combustor was measured for each coal using the sampling and analysis equipment and procedures described earlier. Figures 26 and 27 show the variations in oxygen and carbon dioxide concentrations with height while firing on Eagle Butte and Robinson coal, respectively, at 200,000 Btu/hr.

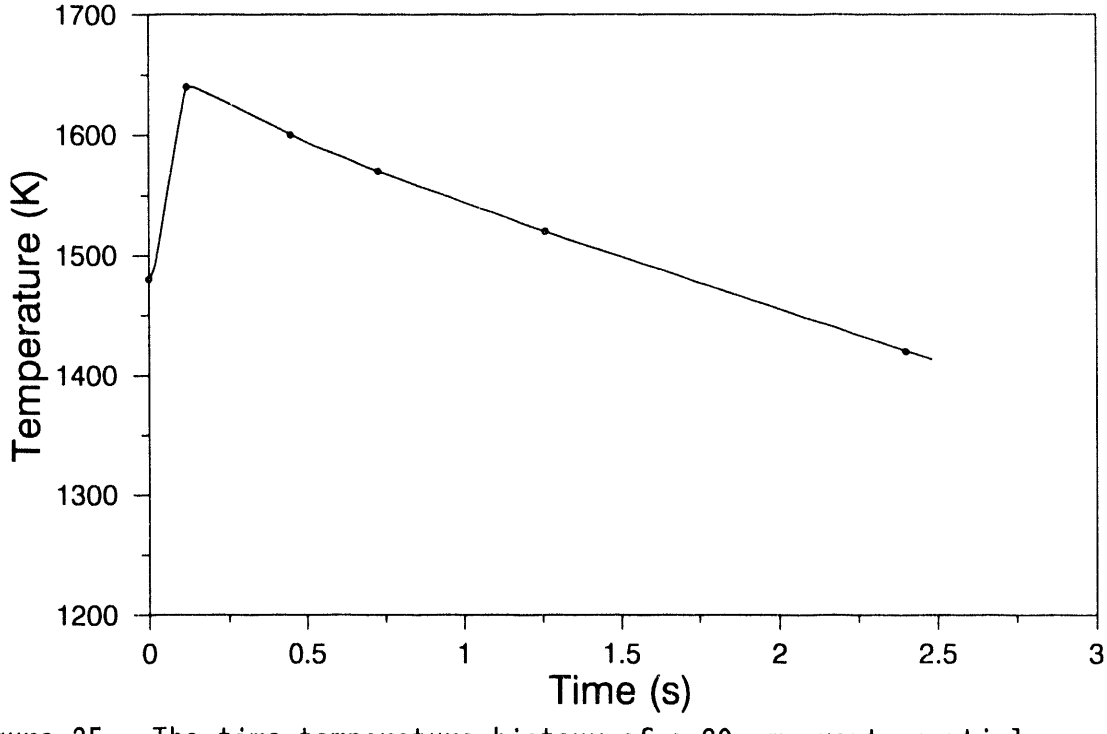

Figure 25. The time-temperature history of a 20-μm quartz particle as it passes from Port 1 to Port 10.

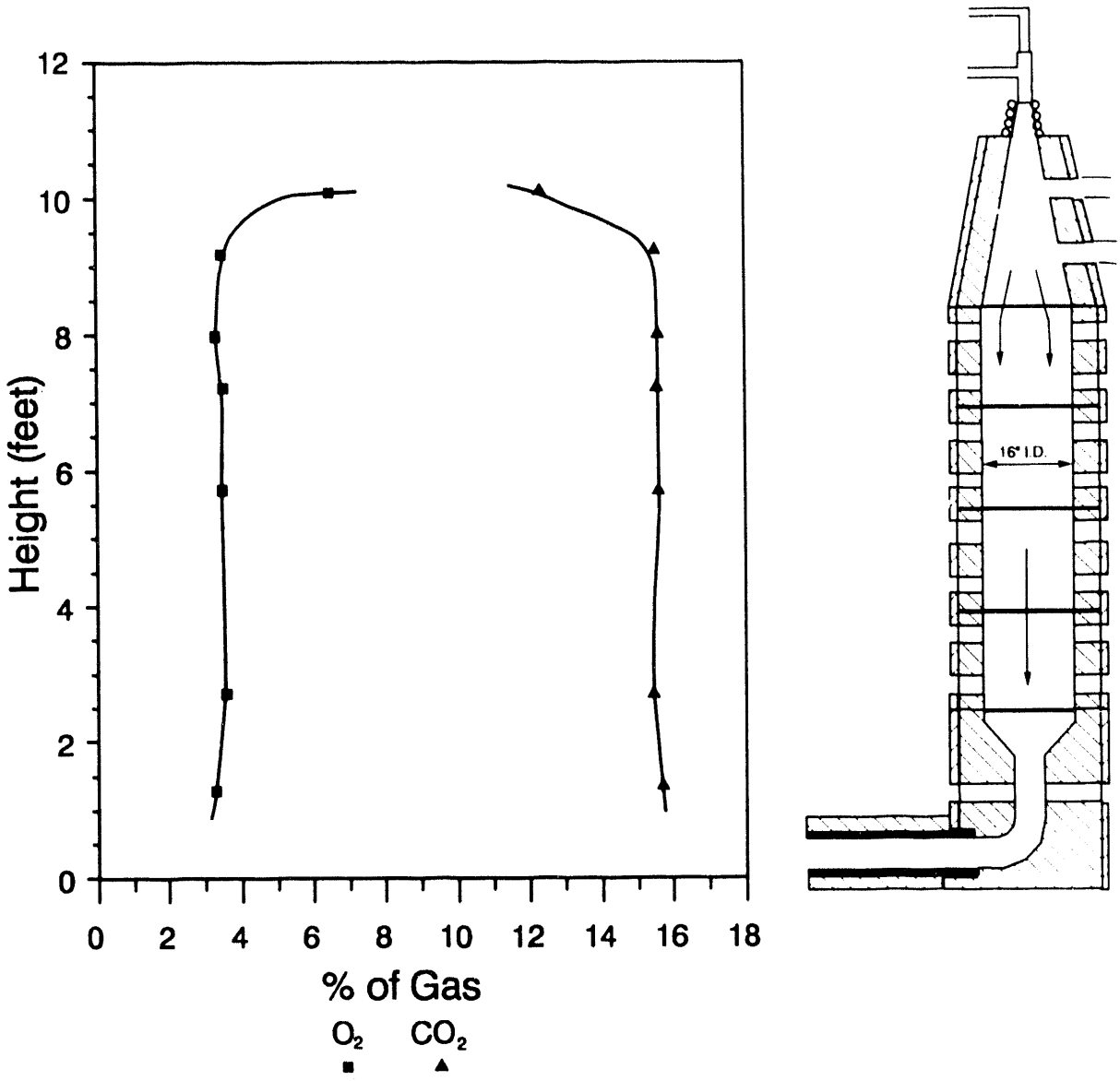

Figure 26. Oxygen and carbon dioxide concentrations versus height while firing Eagle Butte coal at 200,000 Btu/hr.

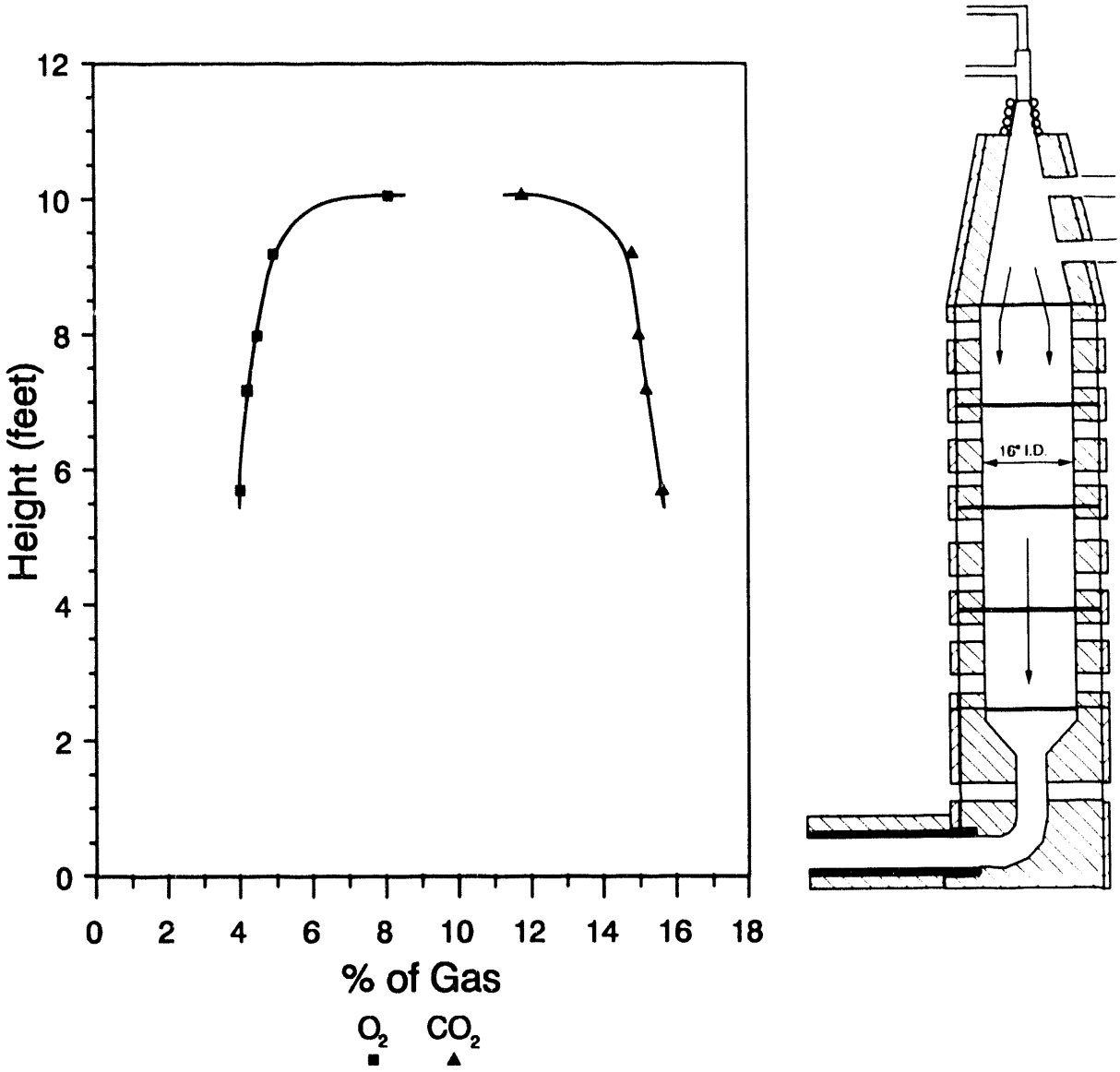

Figure 27. Oxygen and carbon dioxide concentrations versus height while firing Robinson coal at 200,000 Btu/hr.

As can be seen from Figures 26 and 27, the oxygen and carbon dioxide concentrations in the combustor gas reach stable values by the time the coal particles reach the second port from the top, implying that most of the combustion of the coal is complete by this point. This position coincides with the position of the highest gas temperatures. However, visual observations of the flame show that some flame is visible (hence, combustion is occurring) at the level of Ports 3 and 4.

Figures 28 and 29 show the variations with height in the concentrations of sulfur dioxide, nitrogen oxides, and carbon monoxide. The concentration of sulfur dioxide appears to reach a maximum at the fourth port from the top of the combustor for the Eagle Butte coal and at the second port from the top for the Robinson coal. Unfortunately, the readings tended to drift by up to 50%, which makes the exact location of a sulfur dioxide maximum difficult to pinpoint. The sulfur dioxide maximum measured concentrations of 78 ppm for Eagle Butte and 560 ppm for the Robinson are much less than the calculated maximum concentrations of 440 ppm for the Eagle Butte and 880 ppm for the Robinson. This implies that much of the sulfur is present in the combustor in other forms, possibly in condensed phases.

3.8 Results and Discussion of the Analyses of the Particulate Samples

3.8.1 Changes in Aerodynamic Diameter

Table 13 lists the actual volumetric flow rates through the sampling system for each test as well as the aerodynamic cutpoint for each cyclone under the sampling conditions. Table 14 lists the actual physical D_{50} for each cyclone as compared to the specific gravity of a given particle.

The total weight of particulate matter collected in the multicyclone system and recovered from the sampling probe for each combustion test is listed in Table 15. The amounts collected in each cyclone in the multicyclone, the filter, and the inside of the interchangeable water-cooled sampling head on the particulate sampling probe are listed as percents of the total collected. The coal data was gathered by thinly dispersing a sample of each coal on a plate and sucking it through the multicyclone system using flow rates comparable to those used when sampling at Port 2 in the combustor.

No filter was used when sampling at the second port during the combustion tests of the Robinson coal because it clogged quickly and did not allow a sample large enough for analysis to be collected in the cyclones. In general, it was found that the relative amount of particulate sample collected in the first cyclone decreased as the sampling point moved down the combustor. The decrease in the amount collected in the first cyclone was made up for by relative increases in the amounts collected in the second and third cyclones. The amount collected on the filter did not show a clear trend. The changes in amounts collected showed that the aerodynamic diameter of the particles decreased as combustion progressed. The decrease in aerodynamic size during combustion can have several causes. The larger particles may be breaking up during combustion, causing the overall size distribution of the particles to shift to smaller sizes. In effect, combustion of the organic fraction of the

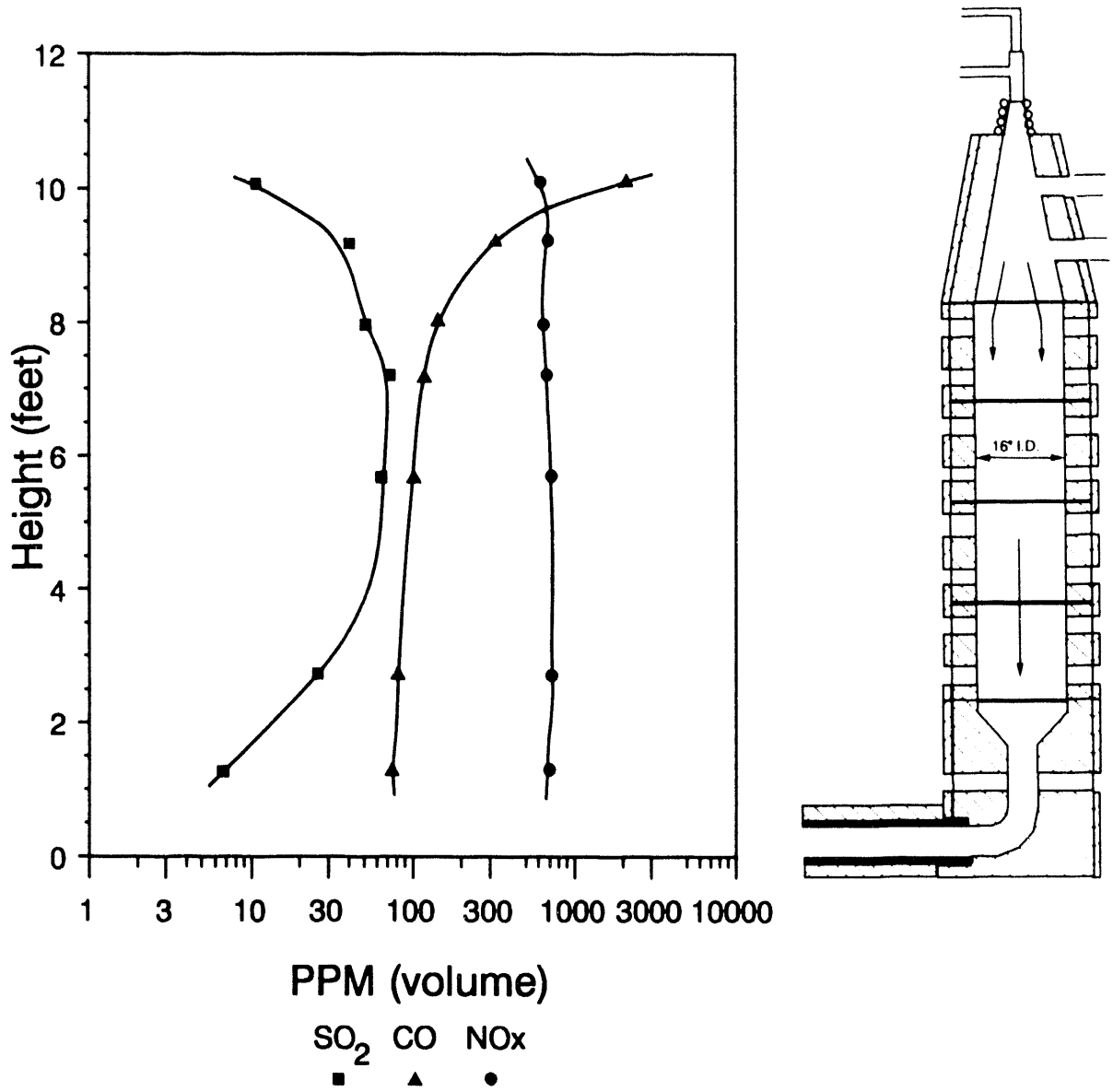

Figure 28. Sulfur dioxide, nitrogen oxides, and carbon monoxide concentrations versus height while firing Eagle Butte coal at 200,000 Btu/hr.

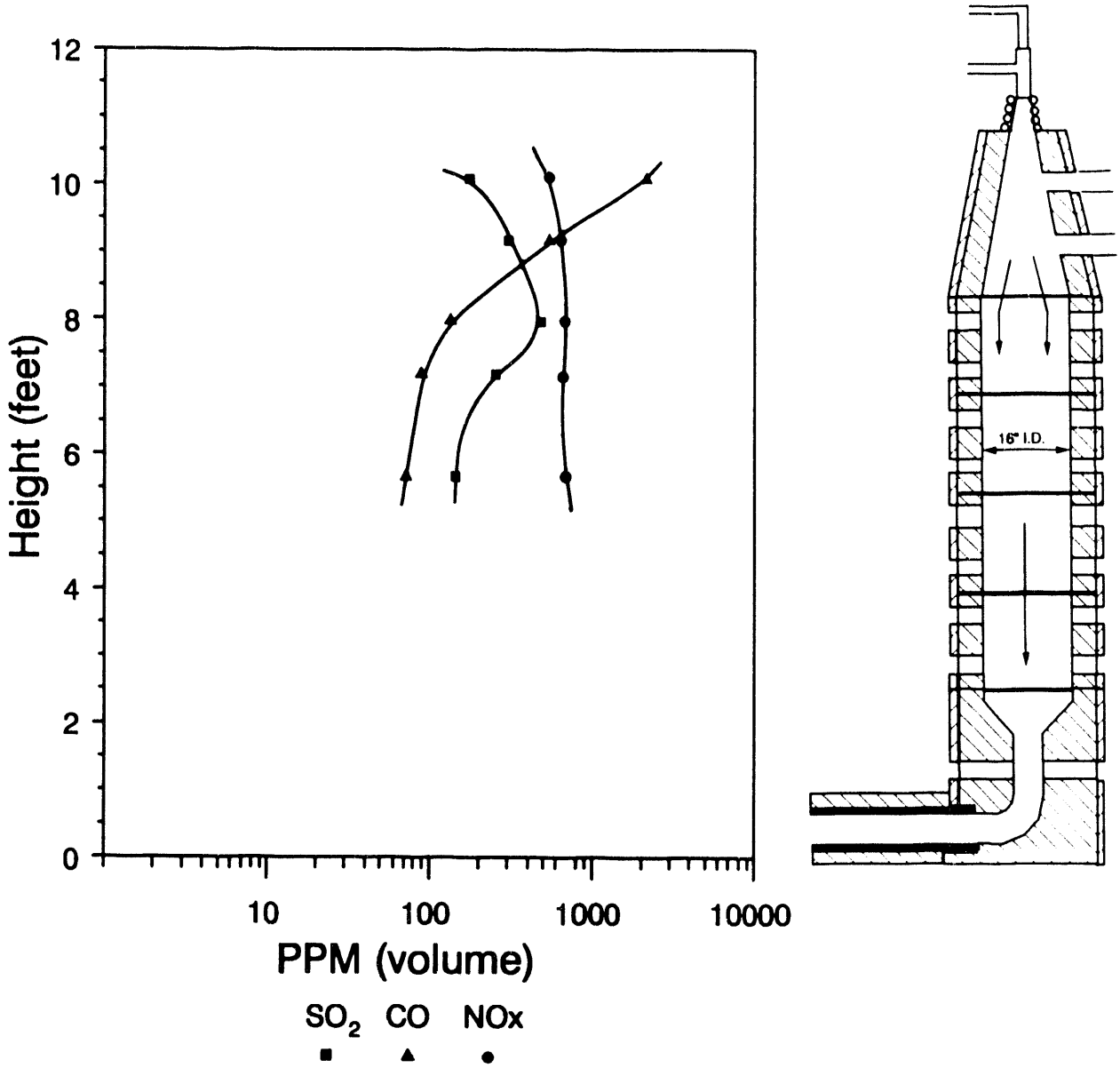

Figure 29. Sulfur dioxide, nitrogen oxides, and carbon monoxide concentrations versus height while firing Robinson Seam coal at 200,000 Btu/hr.

TABLE 13

ACTUAL VOLUMETRIC FLOW RATES AND CYCLONE D_{50} VALUES USED DURING PARTICULATE SAMPLING

Sample	Sampling Rate $(cfm)_{90c}$	Cyclone Cutpoints (μm) 1	2	3
Eagle Butte Port 1	0.75	~15	3.6	0.71
Eagle Butte Port 2	0.69	~15	4.0	0.80
Eagle Butte Port 10	0.99	~13	2.9	0.55
Robinson Port 1	0.83	~14	3.4	0.66
Robinson Port 2	0.75	~15	3.6	0.71
Robinson Port 10	1.08	~13	2.3	0.50
Average	0.85	~14	3.3	0.66

TABLE 14

AVERAGE PHYSICAL D_{50} VERSUS SPECIFIC GRAVITY

Cyclone Number	Aerodynamic D_{50} (μm)	Actual D_{50} (μm) for Specific Gravity 1.0	1.3	2.6	5.2
1	~13	13	11.4	8.1	5.7
2	~ 3.3	3.3	2.9	2.0	1.4
3	~ 0.66	0.66	0.58	0.41	0.29

TABLE 15

AMOUNT OF PARTICULATE MATTER COLLECTED IN EACH SAMPLING SYSTEM STAGE

	Cyclone					
	1(%)	2(%)	3(%)	Filter (%)	Probe (%)	Total (g)
Eagle Butte						
Coal	92.4	6.2	1.4	0.0	n.c.	18.864
Port 1	82.6	11.3	4.7	1.0	0.4	18.555
Port 2	76.6	12.3	7.3	1.3	2.5	4.700
Port 10	74.0	16.4	6.7	0.4	2.4	5.512
Robinson						
Coal	95.4	3.8	0.8	0.0	n.c.	28.841
Port 1	88.1	8.1	3.3	0.5	n.c.	23.867
Port 2	83.5	11.5	5.0	n.c.	n.c.	9.923
Port 10	77.9	15.2	5.8	0.1	1.0	9.816

n.c. - Not Collected.

coal can be thought of as a continual degradation of size of the organic particles until, at 100% burnout, the aerodynamic size distribution of the sample is that of the remaining ash. Because the particulate sample collected at Port 10 shows essentially complete burnout, and because the aerodynamic size distribution of the Port 10 samples is smaller than that of the original coal, then the aerodynamic size distribution of the ash is less than that of the original coal.

3.8.2 Proximate Analyses

In Section 3.7.2.3, calculations are shown and a figure given of the time-temperature history of extraneous inorganic particles as they traverse the down-fired combustor. This information can be used to give a rough idea of the conditions experienced by the extraneous inorganic particles that may have caused some of the changes in the particles which will be discussed in this chapter. In general, the inorganic particles that were originally embedded in larger coal particles experience higher temperatures because of the exothermic oxidation of the coal.

The degree of burnout versus sampling position was calculated using an ash tracer method with information gained from proximate analyses performed on 10-milligram samples with a thermogravimetric analyzer (TGA). Complete proximate analyses were performed on the TGA (rather than just ash content determinations) so that the variations in volatile matter content with degree of burnout could be determined as well as overall burnout. This information is necessary if determinations of the liberation of organically associated inorganics versus burnout and volatile matter loss are to be made. In making such a comparison, however, it is required that the determined volatile matter content of the sample does not include tars present in the sample.

The tars that may occur in the particulate sample were volatilized from the coal in the combustor and condensed upon cooling in the sample probe. The presence of tars in the samples will cause excess volatile matter to be registered during the proximate analysis of the sample. The effect would be most pronounced for samples collected at positions in which relatively high levels of unburned volatilized matter are present in the combustion gas, most likely at the highest sampling points. Therefore, to determine the actual volatile matter content of the chars, a portion of the bulk particulate samples collected at Ports 1 and 2 were Soxhlet-extracted with toluene for at least 24 hours. As a control, samples of the coals were also extracted. TGA proximate analyses were then performed on the Soxhlet residue to find the true or tar-free volatile matter content of the sample.

Table 16 lists the TGA proximate analyses of the coals, Soxhlet-extracted particulates, bulk samples collected at each sampling position, and individual cyclone samples for the Eagle Butte coal. An error was made in the moisture determination of the coals and Port 1 bulk and Soxhlet-extracted samples, so all volatile matter, fixed carbon, and ash content analyses are listed on a moisture-free basis so that more direct comparisons between the analyses can be made.

The proximate analyses of the Port 1 bulk and Soxhlet residues show insignificant differences in volatile matter content which implies that no significant amount of tars had condensed in the Port 1 samples. The proximate analyses of the Port 2 bulk and Soxhlet residues show an increase in the volatile matter content of the Soxhlet-extracted residues. The increase may be due to a retention of toluene on the residues that evaporates upon heating when determining the volatile matter content of the samples. However, the fixed carbon content of the residues increases by nearly the same percentage as the volatile matter content, whereas the ash content decreases. This implies that the increase in volatile matter and fixed carbon in the Port 2 Soxhlet residues may be caused by a loss of inorganic particulates that make up a portion of the ash in the Port 2 bulk samples. The loss of ash-forming constituents causes an apparent increase in the volatile matter and fixed carbon contents of the residues. This would mask the extraction of condensed tars from the sample, except that the volatile matter content increases relative to the fixed carbon content. The relative increase implies that little condensed tar was removed during the Soxhlet extraction.

TABLE 16

TGA PROXIMATE ANALYSES OF COALS AND PARTICULATE SAMPLES

Sample	H_2O (%)	VM (%MF)	FC (%MF)	Ash (%MF)
Eagle Butte				
Coal	17.0*	45.3	47.5	6.9
Port 1				
Bulk	5.8*	41.4	45.5	13.1
Sox. Res.	4.6*	42.1	46.8	11.1
Cyclone 1	2.7	37.7	50.7	11.6
Cyclone 2	4.6	33.2	47.0	19.8
Cyclone 3	2.6	34.3	42.7	22.8
Port 2				
Bulk	2.1	13.1	20.2	66.6
Sox. Res.	1.8	19.8	26.5	53.8
Cyclone 1	0.4	13.3	24.2	62.6
Cyclone 2	0.4	6.2	1.2	92.5
Cyclone 3	0.3	8.9	-3.1	93.9
Port 10				
Bulk	0.2	2.4	0.4	97.2
Cyclone 1	0.1	2.7	0.9	96.4
Cyclone 2	0.2	1.0	0.0	99.1
Cyclone 3	0.2	6.8	1.1	93.2
Robinson				
Coal	13.4*	37.2	52.0	10.9
Coal				
Sox. Res.	2.9*	38.3	51.9	9.8
Port 1				
Bulk	5.2*	33.6	51.6	14.8
Sox. Res.	4.4*	35.3	51.2	13.5
Port 2				
Bulk	2.4	14.0	29.3	56.7
Sox. Res.	3.2	19.0	37.2	43.8
Port 10				
Bulk	0.2	2.7	0.4	97.0

* Moisture data is low due to incorrect TGA proximate procedure.

A comparison of the volatile matter and fixed carbon contents of the coals and combustor samples shows that volatile matter loss occurs at an initially higher rate than combustion of the fixed carbon. By the time the particulates reach the last sampling port (Port 10), however, the fixed carbon content of the coals has been completely combusted, whereas some volatile matter is remaining in the samples. It is unlikely that the volatile matter in the Port 10 samples is of an organic nature because the time experienced by the particulates at the temperatures present in the combustor should be sufficient to cause the complete devolatilization and combustion of any volatile organic species. Instead, it is more likely that the weight loss detected during the proximate analyses of the Port 10 samples is due to decomposition of carbonates and sulfates (or reduced forms of sulfate) that formed in the cyclones as the combustion gases passed over the particulates during sampling.

Comparisons of the ash contents of the Eagle Butte cyclone samples collected at Ports 2 and 3 show that the smaller particulates exhibit greater levels of burnout than the larger particulates. The greater burnout occurs because the smaller particles have a greater diffusion-controlled, heterogeneous burning rate than the larger particles and so will burn out more quickly than the larger particles. This trend does not hold for loss of volatile matter because the samples collected in the most efficient cyclone (Cyclone 3) exhibit higher volatile matter contents than the Cyclone 2 samples. If the volatile matter emitted by the samples was organic, then lower levels would be expected to be emitted from the Cyclone 3 samples because the smaller Cyclone 3 particles would have undergone a higher relative volatile matter loss in the combustor as compared to the larger Cyclone 2 samples (18). This may be caused by the formation of carbonate or sulfates (or reduced forms) in the cyclone during sampling as the combustion gases pass over the samples. The Cyclone 3 samples would exhibit higher levels of capture than the Cyclone 2 samples because of the higher surface area to volume ratio of the smaller particles captured by Cyclone 3. In addition, the Cyclone 3 samples contain relatively more sodium than the Cyclone 2 samples. Since sodium forms relatively more volatile carbonate and sulfate species (or their reduced forms) than the other major elements present, a higher relative weight loss could be expected from the Cyclone 3 samples due to decomposition during the proximate test.

Evidence that reduced forms of the more common compounds exist in some of the samples can be seen in the proximate data for the Cyclone 3 sample collected at Port 2. The data shows a negative fixed carbon content of the samples. The fixed carbon content is determined by cooling the devolatilized sample from 950°C to 750°C and then switching to oxygen or air as a purge gas. When analyzing coal by this method, a weight loss is determined that is interpreted as due to the combustion of the carbon in the sample, leaving a noncombustible residue that is termed ash. The fixed carbon content is defined as the change in weight of the sample due to the oxidation step. The Eagle Butte Port 2 Cyclone 3 sample exhibits a negative fixed carbon content because the weight of the sample showed a net increase upon the introduction of the oxygen to the system. The net weight increase implies that some of the inorganic matter must have been present in a reduced state that became fully oxidized upon the addition of the oxygen. Also, the weight gain was greater than the weight loss caused by the combustion of any remaining carbon.

3.8.3 Inorganic Composition of the Coals

The size and composition of the inorganic fraction of the coals was determined with several techniques. The inorganic elemental composition was found using lithium metaborate fusion of the ASTM ash followed by dissolution and direct current plasma spectrometry. Sulfur contents were determined with a Leco sulfur analyzer. A qualitative determination of the crystalline phases present was performed by x-ray diffraction. The size distribution and relative quantities of inorganic particles with diameters greater than 1.0 μm were determined by CCSEM. A qualitative description of the inorganic particles with diameters less than 1.0 μm was performed by TEM in conjunction with energy-dispersive x-ray analysis. However, not all of the analyses of the Robinson samples are complete, so only the analyses of the inorganic compositions of the Eagle Butte samples will be discussed in this report.

3.8.3.1 Eagle Butte Coal

Elemental. The inorganic elemental contents of the ASTM ashes of the cyclone-separated Eagle Butte coal are listed in Table 17. They are listed on an oxide basis. The metal oxides have been normalized to total 100% on an SO_3-free basis. The SO_3 numbers were normalized with the other metal oxides.

There are three significant trends in the inorganic element concentration versus coal particle-size data shown in Table 17. First, the concentration of silicon in the samples decreases as the particle size decreases. Chemical fractionation data reported elsewhere (19) shows that the silicon in samples taken from the same lot of Eagle Butte coal is present in the coal in a non-ion exchangeable, non-acid leachable form that is probably quartz. The composition versus size data then implies that the quartz is concentrated relative to the other elements in the larger size fractions of the bulk coal. Second, the concentration of aluminum increases relative to the other elements in the coal as the particle size decreases. The chemical fractionation analyses of a similar sample of Eagle Butte (19) shows that about two-thirds of the aluminum is present in a non-acid leachable form, probably clays, whereas one-third of the aluminum is present in an acid leachable form, possible in organic coordination complexes. Because the amounts of aluminum in the two forms are similar, however, it is difficult to tell whether the increase in aluminum relative to other elements in the coal as the particle size increases is caused by an increase in the amount of clays or aluminum coordination complexes with a decrease in particle size. Finally, the concentration of iron decreases relative to the other elements as the particle size decreases. The chemical fractionation data (19) shows that approximately 80% of the iron is present in an acid leachable form, possibly siderite or organic coordination complexes. Since the relative concentration of iron decreases by 40% from the largest coal particles to the smallest, then the concentration of acid leachable iron must decrease as the particle size of the coal decreases.

Crystalline. A sample of the bulk Eagle Butte coal was analyzed by x-ray diffraction (XRD) to determine qualitatively the crystalline phases present. Typically coal is ashed at low temperatures before XRD analysis to increase the signal to noise ratio in the XRD pattern. However, some

TABLE 17

INORGANIC ELEMENTAL COMPOSITION OF EAGLE BUTTE CYCLONE SAMPLES

Elemental Oxide (wt%)	Bulk	Cyclone 1	Cyclone 2	Cyclone 3
Na_2O	2.5	3.0	3.1	2.3
MgO	7.1	6.5	7.8	6.9
Al_2O_3	17.0	15.8	24.2	24.7
SiO_2	32.0	35.7	31.2	27.8
K_2O	0.3	0.2	0.4	1.0
CaO	30.7	28.5	24.0	30.6
TiO_2	1.0	0.9	1.2	1.0
MnO	0.1	0.1	0.1	<0.01
Fe_2O_3	8.0	9.1	7.9	5.5
SO_3	13.3	17.2	n.a.	n.a.

n.a. - Not analyzed due to insufficient amount of sample.

transformations and formation of crystalline phases often occur during low-temperature ashing of low-rank coals. Therefore, no ashing of the coal was performed before XRD analysis was performed.

The XRD pattern of the Eagle Butte coal showed only a quartz peak within a broad amorphous background.

CCSEM. Samples of the bulk coals were analyzed by computer-controlled scanning electron microscopy (CCSEM). From the analysis of known minerals and past experience of the researchers at the University of North Dakota Energy and Environmental Research Center, an initial set of inorganic particle types was defined based on the energy-dispersive x-ray analyses of the particles detected by the CCSEM. The definitions for mineral types identified by CCSEM are listed in Table 18. The x-ray percentages listed in the table are percentages of the total x-ray counts detected for all elements of interest. The elements that were analyzed for are Na, Mg, Al, Si, P, Cl, K, Ca, Ti, Fe, and Ba.

TABLE 18

DEFINITIONS OF INORGANIC PARTICLE TYPES--VALUES ARE PERCENTS OF THE TOTAL X-RAY COUNTS FOR THE ELEMENTS OF INTEREST

Quartz	Al<5, Si≥80
Iron Oxide	Si<10, S<5, Mg<5, Al<5, Fe≥80
Aluminosilicate	K<5, Ca<5, Fe<5, Si>15, Si+Al≥80
Ca-Al-Silicate	S<10, Ca>K, Ca>Fe, Ca>5, Al>10, Si>10, Ca+Al+Si≥80
Fe-Al-Silicate	S<5, Fe>Ca, Fe>K, Fe>5, Si>10, Fe+Al+Si≥80
K-Al-Silicate	K≥Ca, K≥Fe, K≥5, Si≥10, Al≥10, K+Si+Al≥80
Ankerite	S≤15, Mg<Fe, Fe≥20, Ca>20, Ca+Fe+Mg≥80
Pyrite	Ca≤10, 10≤Fe<40, S≥10, Fe+S≥80
Gypsum	Ti=Ba<12, Si<10, S>20, Ca≥20, Ca=S≥80
Barite	Fe<10, Ca≤5, S≥20, Ba+S+Ti≥80
Gypsum/Barite	Fe<5, Ca≥5, Ba≥5, Ti≥5, S≥20, Ca+Ba+Ti+S≥80
Apatite	P≥20, Ca≥20, Ca+P≥80
Ca-Silicate	Al≤10, S≤10, Si≥20, Ca≥14, Ca+Si≥80
Gyp/Al-Silicate	Al≥5, Si≥5, S≥5, Ca>5, Ca+S+Al+Si≥80
Ca-Aluminate	S≤10, Si≤10, Al≥15, Ca≥20, Ca+Al≥80
Spinel	Ca<5, Si<5, Al≥5, Al+Mg+Fe≥80
Alumina	Al≥80
Calcite	S<10, Mg>5, Si<5, P<15, Ti<5, Ba<5, Ca>80
Rutile	S<5, Ti + Ba≥80
Dolomite	Mg>10, Ca>10, Ca+Mg≥80
Pyrrhotite/$FeSO_4$	10≤S<40, Fe+S≥80
KCl	K≥30, Cl≥30, K+Cl≥80
Ca-Rich	65≤Ca<80
Si-Rich	65≤Si<80
Unknown	All other compositions

Because no atomic number, absorption, or fluorescence (ZAF) corrections were used, it was necessary to make some definitions relatively broad. Some overlap appears in the definitions of the Ca-rich and Si-rich inorganic types and other inorganic types that contain high levels of Ca or Si. The overlap does not pose a difficulty in assigning types because the Ca-rich and Si-rich categories appear at the end of the program. Since the program checks the composition of a particle against the definitions in the sequence listed, the Ca-rich and Si-rich categories are assigned only if the composition of the particle does not first meet the criteria of the other inorganic types in the list. The categories of gypsum/barite and gypsum/aluminosilicate were defined because gypsum has been found to occur intergrown with barite and aluminosilicate particles.

Table 19 lists by average diameter the relative area percents of the inorganic particles found in the Eagle Butte coal by CCSEM analysis. The size ranges that the particles are listed in are a geometric progression differing by a factor of the cube root of 10. A geometric size distribution was used to lessen the effects of sectioning that cause the exposed cross sections of the

TABLE 19

THE RELATIVE AREA PERCENTS OF THE INORGANIC PARTICLES IN EAGLE BUTTE COAL

Average Diameter (μm)	1.0-2.2	2.2-4.6	4.6-10	10-22	22-46	>46	Total
Quartz	0.5	1.4	2.5	24.4	36.7	13.4	78.9
Iron Oxide	0.0	0.0	0.0	0.6	0.0	0.0	0.7
Aluminosilicate	0.1	0.3	0.4	3.3	5.9	0.0	9.9
Ca-Al-Silicate	0.1	0.1	0.0	0.0	0.0	0.0	0.2
Fe-Al-Silicate	0.0	0.0	0.0	0.0	0.0	0.0	0.1
K-Al-Silicate	0.0	0.0	0.0	0.3	0.0	0.0	0.3
Ankerite	0.0	0.0	0.0	0.0	0.0	0.0	0.0
Pyrite	0.0	0.0	0.0	0.9	0.0	0.0	0.9
Gypsum	0.0	0.0	0.0	0.0	0.0	0.0	0.0
Barite	0.0	0.0	0.0	0.0	0.0	0.0	0.0
Gypsum/Barite	0.0	0.0	0.0	0.0	0.0	0.0	0.0
Apatite	0.0	0.0	0.0	0.0	0.0	0.0	0.0
Ca-Silicate	0.0	0.0	0.0	0.2	0.0	0.0	0.2
Gyp/Al-Silicate	0.0	0.0	0.0	0.0	0.0	0.0	0.0
Ca-Aluminate	0.0	0.0	0.2	0.0	0.0	0.0	0.2
Spinel	0.0	0.0	0.0	0.0	0.0	0.0	0.0
Alumina	0.1	0.1	0.0	0.0	0.0	0.0	0.1
Calcite	0.0	0.0	0.0	0.0	0.0	0.0	0.1
Rutile	0.0	0.0	0.0	0.0	0.0	0.0	0.0
Dolomite	0.0	0.0	0.1	0.0	0.0	0.0	0.1
Pyrrhotite/$FeSO_4$	0.0	0.0	0.0	0.0	0.0	0.0	0.0
KCl	0.0	0.0	0.0	0.0	0.0	0.0	0.0
Ca-Rich	0.0	0.0	0.0	0.0	0.0	0.0	0.1
Si-Rich	0.1	0.2	0.0	2.5	0.0	0.0	2.8
Unknown	0.2	0.2	0.4	2.3	2.1	0.0	5.1
Total	1.1	2.3	3.6	34.5	44.7	13.4	99.6

particles to be less than or equal to the maximum diameter of the particles (20,21). In effect, the use of a geometrical size distribution makes the errors related to sectioning similar in magnitude to the errors related to the counting statistics. Therefore, no corrections for shifting of particle diameters to smaller size ranges caused by sectioning are applied to the data.

The data in Table 19 shows that the majority of the area of inorganic particulates with average diameters greater than 1.0 μm are quartz particles with average diameters between 10 and 46 μm. In all, over three quarters of the volume of the inorganic particles detected are quartz particles. Approximately 10% of the area of inorganic particles detected fell into the aluminosilicate category, with the majority also falling into the 10- to 46-μm average diameter range. The low levels of inorganic particles that contain calcium, iron, or magnesium imply that those elements are predominantly present in the coal in organic associations or as submicron inorganic particles.

TEM. TEM analyses of 0.1-μm thick ultrathin sections of the Eagle Butte coal showed two main types of coal particles. One type, shown in Figure 30, exhibits a relatively uniform level of contrast with only small amounts of high-contrast inclusions. The other type of coal particle, pictured in Figure 31, contains high levels of small, high-contrast particles with circular cross sections. It is estimated that four times as many coal particles were observed with low levels of inclusions as coal particles with high levels of inclusions. Both types of coal particles also contain larger, irregularly shaped mineral grains.

The small inclusions with circular cross sections occur in three size ranges. The smallest particles have diameters of approximately 2×10^{-3} to 3×10^{-3} μm. They are approximately 0.1 millimeters in diameter in the 49,000x photos shown in Figures 30 and 31 and are evenly dispersed. They are most clearly seen in the thin regions of the coal and the embedding resin. Some particles also appear to have floated off of the coal and into the resin. The particles never occur in the resin more than approximately 0.5 μm from a coal or char particle, however. A second size class of the high-contrast inclusions with circular cross sections has diameters between 2×10^{-2} and 3×10^{-2} μm. In Figure 31 this size class is seen as particles with diameters of 0.9 to 1.5 millimeters in diameter. They do not appear to be as evenly dispersed across the coal particles as the smallest size range. The largest size class is composed of particles with diameters greater than approximately 6×10^{-2} μm in diameter, although this size range is not as distinct from the middle size range (i.e., there is some gradation between them).

The composition of the particles is difficult to discern. By operating in scanning TEM mode, a sufficiently small electron spot can be produced so that individual particles of the smallest size range can be illuminated, thereby partially isolating the source of x-rays detected by the energy-dispersive x-ray spectrometer (EDS) to a volume of sample that includes only one particle. Unfortunately, there is a tradeoff in beam current that must be made due to the effects of background noise in the EDS signal and beam damage suffered by the sample. In practice, to prevent beam damage, the beam current had to be so low that the signal to noise ratio in the EDS signal was minimal. However, using counting times of several minutes, a signal did emerge in the EDS spectra of individual small particles or groupings of them. For the Eagle Butte coal, the signal usually showed the presence of calcium, iron, and sulfur. The source of the calcium, sulfur, and iron signals is obscured by the fact that all three elements are known to be associated directly with the organic portion of the coal. Since the ultrathin section is approximately 1×10^{-1} μm thick and the smallest particles are 2×10^{-3} μm in diameter, it is impossible to tell if the x-ray signal is emitted from the coal or the particles. In general, it was found that clear x-ray signals could only be obtained from particles that had diameters above several hundredths of a micron, although some smaller particles gave strong x-ray signals if they were composed of high atomic number elements.

The possibility exists that the small particles which do not give strong x-ray signals may not be inorganic. Friel et. al., (22) have shown the formation of mesophase spheres upon heating of several bituminous coals. The

Figure 30. TEM photograph (49,000x) of an Eagle Butte coal particle containing low levels of high-contrast inclusions.

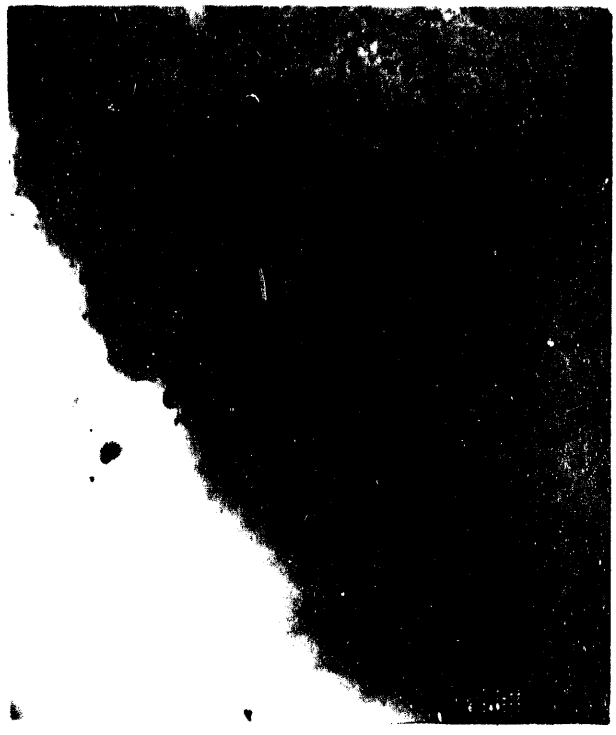

Figure 31. TEM photograph (49,000x) of an Eagle Butte coal particle containing high levels of high-contrast inclusions.

spheres they reported have the size and appearance of the medium-size high-contrast inclusions shown in Figure 32. Several lines of evidence support the conclusion that the small inclusions shown in Figure 32 are not similar mesophase spheres. First, the coal had not been heated prior to analysis. Since mesophase usually forms on heating, one would not expect mesophase spheres to be present in the coal. However, some heating of the sample may have occurred in the TEM through absorption of energy from the electron beam.

Second, the Eagle Butte and Robinson coals are subbituminous coals. Subbituminous coals do not usually form mesophase upon heating. Third, and most convincingly, a close examination of the boundary between the coal particles and the resin shows that some of the smallest particles have separated a small distance from the coal and resided in the resin. Mesophase spheres would not be expected to so easily separate from the coal.

The inorganic particles that did give stronger x-ray signals exhibited elemental ratios similar to the elemental ratios found in commonly occurring coal minerals such as kaolin, quartz, pyrite, and gypsum. In addition, as has been found in other TEM studies of coal (23), relatively large numbers of the smallest particles that gave strong x-ray signals showed concentrations of elements such as are found in rutile (high titanium) and barite (high barium and sulfur). Figure 32 is a TEM photograph (82,000x) of a cluster of particles containing high levels of titanium. Since electron diffraction analysis of the particles was not performed, the mineral types of the particles showing strong x-ray signals cannot be determined definitely. Indeed, electron diffraction studies of coal minerals (24) have shown the existence of the rutile polymorphous anatase and brookite in other coals.

3.8.3.2 Robinson Coal

Elemental. The inorganic elemental contents of the ASTM ashes of the cyclone-separated Robinson coal are listed in Table 20. They are listed on an oxide basis and have been normalized to total 100% on an SO_3-free basis. The SO_3 numbers were normalized to total 100% with the other metal oxides.

Table 20 shows that, as is true for the Eagle Butte coal, the concentration of aluminum increases and the concentration of iron decreases relative to the other elements as the particle size decreases. Unlike the Eagle Butte coal, calcium shows a higher concentration in the smaller particle sizes relative to the larger.

Samples of the bulk coals were analyzed by x-ray diffraction (XRD) to determine qualitatively the crystalline phases present. Typically in XRD analysis of coals, the coal is ashed at low temperatures before x-ray diffraction analysis to increase the signal to noise ratio in the XRD pattern. However, some transformations and formation of crystalline phases often occurs during low-temperature ashing of low-rank coals. Therefore, no ashing of the Eagle Butte or Robinson coals was performed before x-ray diffraction (XRD) analysis was performed.

The XRD pattern of the Robinson coal also showed only a quartz peak within a broad amorphous background signal.

Figure 32. TEM photograph (82,000x) of a cluster of particles in an Eagle Butte coal containing high levels of titanium.

TABLE 20

INORGANIC ELEMENTAL COMPOSITION OF ROBINSON CYCLONE SAMPLES

Elemental Oxide	Bulk	Cyclone 1 (%)	Cyclone 2 (%)	Cyclone 3 (%)
Na_2O (%)	4.7	5.1	1.6	2.3
MgO (%)	3.5	3.2	2.5	1.7
Al_2O_3 (%)	17.4	16.4	29.1	36.4
SiO_2 (%)	40.8	41.9	43.6	41.7
K_2O (%)	0.4	0.2	0.3	0.4
CaO (%)	19.6	19.5	17.6	13.3
TiO_2 (%)	0.7	0.8	0.5	0.4
MnO (%)	<0.05	0.2	0.1	0.1
Fe_2O_3 (%)	12.9	12.9	4.8	3.7
SO_3 (%)	16.7	19.2	n.a.	n.a.

n.a. - not analyzed

CCSEM. Samples of the bulk coals were analyzed by computer-controlled scanning electron microscopy (CCSEM) using the technique and equipment described in the Task 1 section of this report. Care must be taken in interpreting the data because the SEM provides only elemental composition data and not crystallographic data. In addition, no atomic number, absorbance, or fluorescence (ZAF) corrections were applied to the data so the definitions are broad. Therefore, although the inorganic particle types have compositions similar to the defined mineral types, the particles may not have exactly the same crystallographic properties or exact composition as the defined mineral type.

Table 21 lists the CCSEM data for the Robinson coal. The x-ray percentages listed in the table are percentages of the total x-ray counts detected for all elements of interest. The elements that were determined are Na, Mg, Al, Si, P, Cl, K, Ca, Ti, Fe, and Ba.

The data in the table shows that, in contrast to the Eagle Butte coal, the inorganic particle type exhibiting the greatest area concentration (40% of the total) is pyrite. The majority of the pyrite is concentrated in particles with average diameters of greater than 46 μm, with most of the rest in the 10-46 μm range. The only other inorganic particle types that constitute significant fractions of the inorganic particles are quartz and aluminosilicate particles that each make up just over 20% of the total mineral area analyzed. As was true for the Eagle Butte coal, the majority of the quartz in the Robinson coal is present in particles with average diameters of between 10 and 46 μm. The aluminosilicate particles show a similar size distribution but with slightly higher concentrations in the other size categories. As was also true with the Eagle Butte coal, the concentrations of inorganic particles that contain significant levels of Na, Mg, or Ca are minor, implying that those elements are predominantly associated in the coal in organic associations or submicron mineral matter.

Chemical fractionation analysis of a sample of the Robinson coal taken from the same lot as the coal used in the present research shows that, indeed, the majority of the Na, Mg, and Ca are ion-exchangeable with 1 molar NH_4OAc and are therefore most likely present as salts of carboxylic acid groups. Table 22 lists a portion of the chemical fractionation results reported in the CIT annual report for 1989 (19).

TEM. Like the Eagle Butte coal, the Robinson coal showed two main types of coal particles with respect to fine structure, i.e., those with high levels of small, high-contrast inclusions and those with low levels of the inclusions. The inclusions appeared to belong to distinctive size classes similar to those in the Eagle Butte coal, although the sizes of the inclusions in the Robinson coal were approximately 10-20% larger and showed a more dispersed size distribution within each size category. Figure 33 shows a concentration of the smallest inclusions within a Robinson coal particle.

In addition to the smallest high-contrast inclusions, more massive minerals that are known to commonly exist in coals were also seen (as they were in the Eagle Butte ultrathin sections). Figure 34 shows a Robinson coal particle that contains large numbers of massive mineral particles which can be

TABLE 21

THE RELATIVE AREA PERCENTS OF THE INORGANIC PARTICLES IN ROBINSON COAL

Average Diameter (μm)	1.0-2.2	2.2-4.6	4.6-10	10-22	22-46	>46	Total
Quartz	0.1	0.2	0.3	9.9	12.2	0.0	22.7
Iron Oxide	0.0	0.0	0.0	0.0	0.0	0.0	0.0
Aluminosilicate	0.5	1.0	1.3	8.4	7.8	2.6	21.6
Ca-Al-Silicate	0.0	0.0	0.0	0.1	0.0	0.0	0.2
Fe-Al-Silicate	0.0	0.0	0.0	0.0	0.0	0.0	0.0
K-Al-Silicate	0.0	0.0	0.1	0.2	0.0	0.0	0.3
Ankerite	0.0	0.0	0.0	0.0	0.0	0.0	0.0
Pyrite	0.0	0.1	0.1	7.4	10.4	21.8	39.9
Gypsum	0.0	0.0	0.0	2.5	0.0	0.0	2.5
Barite	0.0	0.0	0.0	0.1	0.0	0.0	0.1
Gypsum/Barite	0.0	0.0	0.0	0.0	0.0	0.0	0.0
Apatite	0.0	0.0	0.0	0.0	0.0	0.0	0.0
Ca-Silicate	0.0	0.0	0.0	0.0	0.0	0.0	0.0
Gyp/Al-Silicate	0.0	0.0	0.0	0.0	0.0	1.4	1.4
Ca-Aluminate	0.0	0.0	0.0	0.0	0.0	0.0	0.0
Spinel	0.0	0.0	0.0	0.0	0.0	0.0	0.0
Alumina	0.0	0.0	0.0	0.0	0.0	0.0	0.0
Calcite	0.0	0.0	0.0	0.4	1.0	1.3	2.8
Rutile	0.0	0.0	0.0	0.0	0.0	0.0	0.0
Dolomite	0.0	0.0	0.0	0.0	0.0	0.0	0.0
Pyrr./$FeSO_4$	0.0	0.0	0.0	1.0	1.0	0.0	2.0
KCl	0.0	0.0	0.0	0.0	0.0	0.0	0.0
Ca-Rich	0.0	0.0	0.0	0.1	0.0	0.0	0.1
Si-Rich	0.0	0.0	0.0	0.1	0.0	0.0	0.1
Unknown	0.1	0.0	0.1	1.4	4.6	0.0	6.2
Total	0.8	1.5	2.0	31.6	37.0	27.1	100.0

TABLE 22

CHEMICAL FRACTIONATION RESULTS OF ROBINSON COAL

	Removed by H_2O (%)	Removed by NH_4OAc (%)	Removed by HCl (%)	Remaining (%)
Na	48	60	0	-8[a]
Mg	1	72	7	20
Al	0	0	13	87
Si	1	0	1	98
Ca	0	75	21	4
Fe	0	0	21	79

a - More Na was measured in the extracts than was measured in the original coal.

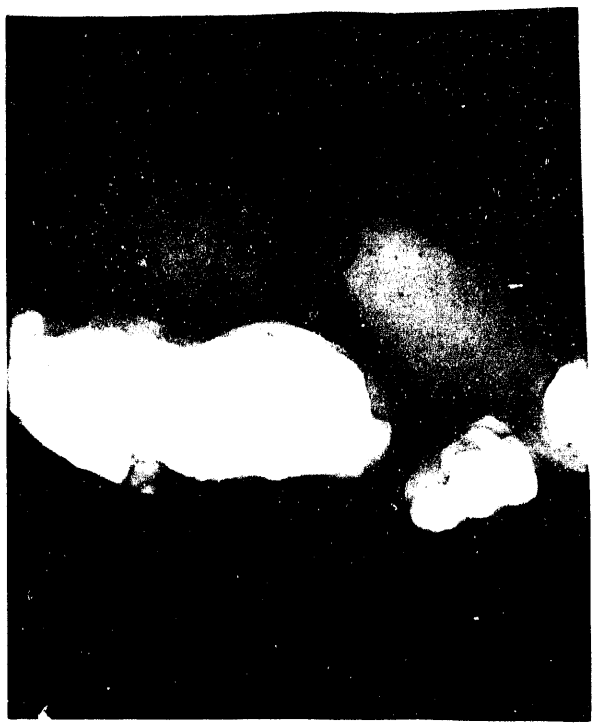

Figure 33. TEM photograph (82,000x) of an ultrathin section of a Robinson coal particle showing large numbers of 4-5-μm diameter high-contrast inclusions. The white areas are holes in the particle that allow the electrons to pass through without absorption.

Figure 34. TEM photograph (3,300x) of an ultrathin section of a Robinson coal particle showing massive mineral inclusions.

seen in the figure as darker areas within the lighter coal matrix. Most of the minerals in this photograph contained high levels of calcium as well as lower concentrations of silicon, sulfur, and iron. The very dark circular area near the bottom of the figure is due to beam damage that occurred while the beam was focused on a cluster of titania particles. As was true in the case of the Eagle Butte coal, the Robinson coal exhibited a concentration of titania particles in the submicron size ranges.

3.9 Inorganic Composition of the Port 1 Particulate Samples

3.9.1 Eagle Butte Port 1

Elemental. By the time the Eagle Butte particulates reached the sampling probe at Port 1, the bulk coal had undergone 50.8% burnout. The residence time of the particles in the radiant zone cannot be calculated exactly due to a lack of gas temperature data above Port 1. However, an estimate of the residence time in the refractory-lined portion of the quarl (using average temperatures and chamber cross sections) is 0.07 seconds. The maximum equilibrium temperature experienced by an extraneous inorganic particle before sampling is approximately 1220°C.

The inorganic elemental contents of the ASTM ashes of the cyclone-separated Eagle Butte particulates collected at Port 1 of the combustor are listed in Table 23. They are listed on a metal oxide basis. The metal oxides have been normalized to total 100% on an SO_3-free basis to make comparisons with the coal data easier. The SO_3 numbers are given on a basis normalized with the other elemental oxides. Because the filter sample was too small for separate analysis, a portion of it was mixed with the Cyclone 3 sample in an amount proportional to their weights.

The criteria used to delineate significant changes between the inorganic elemental concentrations in the cyclone samples between two different sampling ports are twofold. First, the change in concentration of an element in samples collected in the same cyclone at each port must be greater than 10-15% because, based on experience, this is approximately the level of reproducibility of the analytical procedure. Second, changes in the concentration of an element in one cyclone sample must be made up for by an opposite change in another cyclone since the metal oxides are nonvolatile at the cyclone temperatures, and, therefore, the total mass of an element must be conserved from port to port.

As was true with the coal, the concentration of aluminum is higher, while silicon and iron concentrations are lower in the smaller size fractions of the particulates collected at Port 1. A trend not seen in the coal is that the concentrations of sodium, magnesium, and calcium found in the smaller aerodynamic size particles collected at Port 1 are higher than their concentrations in the Cyclone 1 particles. With the exception of sodium, the largest difference in inorganic elemental compositions is between the particles collected in Cyclone 1 and the particles collected in Cyclone 2. Only sodium shows a significant difference in concentration between the Cyclone 2 particles and the Cyclone 3 particles.

TABLE 23

INORGANIC ELEMENTAL COMPOSITION OF EAGLE BUTTE
PORT 1 CYCLONE SAMPLES

Elemental Oxide	Cyclone 1 (%)	Cyclone 2 (%)	Cyclone 3+F (%)
Na_2O	2.3	2.9	6.0
MgO	6.1	8.2	8.2
Al_2O_3	15.9	20.0	20.9
SiO_2	35.8	25.0	21.0
K_2O	0.2	0.2	0.5
CaO	26.3	35.1	34.8
TiO_2	0.9	1.2	1.1
MnO	0.1	0.1	0.1
Fe_2O_3	12.4	7.3	7.3
SO_3	11.8	7.8	9.4

Crystalline. XRD of the Port 1 Cyclone 1 sample showed a major quartz peak within a large amorphous background signal. No other peaks were obvious in the pattern. The Cyclone 2 sample showed a strong quartz peak and weaker lime and periclase peaks. Compared to the Cyclone 2 sample, the Port 3 plus filter sample showed a weaker quartz peak that was immersed in a strong amorphous background, as well as lime and periclase peaks of the same height as the Cyclone 2 samples, but with a much stronger signal to noise ratio. Although the XRD technique used is nonquantitative in nature, the weaker quartz peak in the Cyclone 3 sample may reflect the lower concentrations of silicon in the smaller sized particles. The higher signal to noise ratio of the lime and periclase peaks reflects the higher burnout of the Cyclone 3 samples.

CCSEM. The results of the CCSEM analyses of the Cyclone 1, Cyclone 2, and Cyclone 3 + filter samples collected at Port 1 during a combustion test of the Eagle Butte coal show that relatively large amounts of inorganic particles (principally quartz) that should have been collected in the first cyclone were carried over and collected in Cyclones 2 and 3. For this reason, comparisons between the CCSEM data for those three cyclone samples will not be made. To make comparisons of the data with the CCSEM analysis of the bulk coal easier, the data from the analyses of the individual cyclone samples have

been combined to give a table showing the calculated inorganic particle-size distributions on a bulk particulate sample basis. The calculated inorganic particle-size distribution of the bulk particulate sample collected at Port 1 during combustion testing of the Eagle Butte coal is shown in Table 24. The values for the table of bulk data were found by multiplying the values in the separate cyclone tables by a fraction equal to the fraction of the total ash that was collected in that cyclone. Only those inorganic particle types that showed total concentrations of at least 0.5% of the total inorganic particle area are shown.

A comparison between the CCSEM analyses of the Eagle Butte coal (Table 19 and the particulate sample collected at Port 1 of the combustor (Table 24) shows that the total area of particulate sample found in each size range does not change significantly from that of the coal up to the level of burnout shown by the particulate sample collected at Port 1 (50.8%). In general, no coalescence of any of the inorganic types up to this level of burnout to produce larger or more compositionally complex species is evident. In addition, no fracturing of the inorganic particles to produce greater percentages of smaller (but greater than 1-μm average diameter) particles is evident.

Two main types of char particles were seen in the Port 1 particulate samples: those that were highly vesicular and those that showed little internal structure. A TEM photograph (3,800x) of an ultrathin section of a vesicular char particle is shown in Figure 35. The dark gray areas are the char, the light gray areas are areas of resin, and the white, rounded areas are holes in the resin, perhaps marking positions where large ash particles were plucked during sectioning.

Plucking during sectioning of spherical ash particles with diameters greater than the section thickness was a constant problem. It occurred for a combination of several reasons. The diamond knife used to make the ultrathin sections was a materials science-grade knife. This meant that although the knife could not make sections as thin as a biological-grade knife could, it did not chip as easily as a biological-grade knife. The relative dullness of the knife meant that a softer embedding medium had to be used than could be used if a biological-grade knife were employed. Finally, because the ash particles are relatively smooth and spherical, the softer embedding medium did not hold the particles immobile during sectioning as a harder medium would have, or more irregular particles would have been held.

3.9.2 Robinson Port 1

Elemental. The criteria used to delineate significant changes between the inorganic element concentrations in the cyclone samples between two different sampling ports are twofold. First, the change in concentration of an element in samples collected in the same cyclone at each port must be greater than 10-15% because, based on experience, this is approximately the level of reproducibility of the analytical procedure. Second, changes in the concentration of an element in one cyclone sample must be made up for by an opposite change in another cyclone since the metal oxides are not volatile at the cyclone temperatures, and, therefore, the total mass of an element must be conserved from port to port.

TABLE 24

THE CALCULATED RELATIVE AREA PERCENTS OF THE INORGANIC PARTICLES IN THE EAGLE BUTTE, PORT 1, BULK PARTICULATE SAMPLE

Average Diameter (μm)	1.0-2.2	2.2-4.6	4.6-10	10-22	22-46	>46	Total
Quartz	0.6	2.5	3.7	25.2	33.1	11.7	76.8
Iron Oxide	0.0	0.1	0.2	0.4	0.0	0.0	0.7
Aluminosilicate	0.1	0.2	0.5	2.6	3.8	0.0	7.2
Ca-Al-Silicate	0.2	0.2	0.1	0.2	0.0	0.0	0.7
Pyrite	0.0	0.0	0.1	0.6	0.0	0.0	0.7
Calcite	0.0	0.2	0.1	0.2	0.0	0.0	0.5
Ca-Rich	0.3	0.9	0.5	0.1	0.0	0.0	1.8
Si-Rich	0.1	0.2	0.1	1.8	0.0	0.0	2.2
Unknown	1.0	1.4	0.7	1.9	2.3	0.0	7.3
Total	2.3	5.7	6.0	33.0	39.2	11.7	97.9

Figure 35. TEM photograph (3,800x) of a highly vesicular char particle collected at Port 1 during an Eagle Butte combustion test.

By the time the particulates reached the sampling probe at Port 1, the Robinson coal had undergone 31.9% burnout. The residence time of the particles in the radiant zone was approximately the same as that calculated for the Eagle Butte combustion test, i.e., 0.07 s. The equilibrium temperature of extraneous, nonreacting inorganic particles at the sampling point is approximately 1210°C.

The inorganic elemental contents of the ASTM ashes of the cyclone-separated Robinson particulates collected at Port 1 of the combustor are listed in Table 25. They are listed on a metal oxide basis. The metal oxides have been normalized to total 100% on an SO_3-free basis to make comparisons with the coal data easier. The SO_3 numbers are given on a basis normalized with the other elemental oxides. Because the filter sample was too small for separate analysis, a portion of it was mixed with the Cyclone 3 sample in an amount proportional to their weights.

Little change is seen in the distribution of K, Ti, Mn, Fe, and S among the different cyclones as compared to the original coal. However, Na, Mg, and Ca showed significant changes in their distribution with small decreases in concentration in the Cyclone 1 samples and increases in the Cyclone 2 and Cyclone 3 samples as compared to the coal samples. Na and Ca showed the largest changes. This shifting in concentration from the larger to smaller aerodynamic sizes may be caused by fragmentation of the minerals that contain the elements, or may indicate volatilization from larger particles followed by recondensation of the elements. The latter case is the most probable since these three elements have been shown by chemical fractionation to be the only major elements that are predominantly organically associated in the Robinson coal (19). Conversely, Al and Si showed a decrease in concentration in the Port 1, Cyclones 2 and 3 samples as compared to the coal, Cyclones 2 and 3 samples. The increase may be because of the increases in the other elements or because of agglomeration of Al and Si containing particles during the first 32% burnout. However, the decreases in concentration in the smaller particles are not accompanied by an appropriate decrease in concentration in the Cyclone 1 sample. Since the needed increase in concentration in the Cyclone 1 sample is small (because it constitutes by far the largest fraction of the total particulate sample), the lack of decrease in the Port 1 sample may be due to sampling or analytical errors.

Crystalline. The XRD of both the Robinson Cyclone 1 and Cyclone 2 samples showed only a quartz peak within a broad amorphous background signal. The XRD of the Cyclone 3 sample showed a similar pattern with the addition of a small periclase peak.

CCSEM. The calculated inorganic particle-size distribution of the bulk particulate sample collected at Port 1 during combustion testing of the Robinson coal is shown in Table 26. The values for the table of bulk data were found by multiplying the values in the separate cyclone tables by a fraction equal to the fraction of the total ASTM ash collected in that cyclone, then adding the prorated values. Only those inorganic particle types that showed total concentrations of at least 0.5% of the total inorganic particle area are shown.

TABLE 25

INORGANIC ELEMENTAL COMPOSITION OF ROBINSON PORT 1 CYCLONE SAMPLES

Elemental Oxide	Cyclone 1 (%)	Cyclone 2 (%)	Cyclone 3+F (%)
MgO (%)	2.9	4.0	3.0
Al_2O_3 (%)	15.5	22.7	26.8
SiO_2 (%)	41.6	36.9	33.9
K_2O (%)	0.2	0.3	0.6
CaO (%)	17.8	24.9	3.0
TiO_2 (%)	0.6	0.7	0.4
MnO (%)	<0.1	<0.1	<0.1
Fe_2O_3 (%)	17.4	5.3	3.4
SO_3 (%)	16.9	17.1	10.8

TABLE 26

THE CALCULATED RELATIVE AREA PERCENTS OF THE INORGANIC PARTICLES IN THE ROBINSON, PORT 1 PARTICULATE SAMPLE

Average Diameter (μm)	1.0-2.2	2.2-4.6	4.6-10	10-22	22-46	>46	Total
Quartz	1.0	2.9	3.9	9.7	13.4	17.9	48.9
Iron Oxide	0.0	0.1	0.0	0.2	0.3	0.0	0.6
Aluminosilicate	1.5	1.4	1.3	7.1	7.7	4.4	23.4
Ca-Al-Silicate	1.2	0.7	0.5	1.2	0.9	0.0	4.4
Pyrite	0.0	0.1	0.1	0.7	0.9	0.0	1.9
Gypsum	0.2	0.2	0.1	0.3	0.0	0.0	0.8
Ca-Silicate	0.1	0.1	0.1	0.0	0.4	0.0	0.7
Gyp/Al-Silicate	0.1	0.1	0.0	0.5	0.3	0.0	1.0
Calcite	0.0	0.1	0.0	0.5	0.9	0.0	1.4
Pyrrhotite	0.0	0.0	0.0	0.1	0.3	0.0	0.4
Ca-Rich	0.4	0.6	0.2	0.2	0.0	0.0	1.4
Si-Rich	0.2	0.3	0.5	0.2	1.1	0.0	2.4
Unknown	1.5	1.1	0.3	2.5	1.6	3.2	10.2
Total	6.4	7.6	7.1	23.2	27.8	25.5	97.6

A comparison of the data in Table 21 and Table 26 shows that changes in the size distribution of the mineral particles in the Robinson coal during the first 30% of burnout included reductions in the concentrations of inorganic particles with average diameters between 10 and 46 μm, mostly due to decreases in the concentration of pyrite in that size range. In addition, increases in the concentrations of inorganic particles with diameters less than 10 microns is also apparent, mostly due to increases in the concentration of quartz particles in that size range. Little change is seen in the concentration of particles in the >46 μm size range, although a shift in particle type within that size range from pyrite to quartz is seen.

The reasons for changes in the concentration of an inorganic particle type within a given size range are diverse. Decreases may be caused by several factors. Fragmentation of an inorganic particle will cause a decrease in size without a change in particle type. Usually fragmentation will manifest itself as a decrease in one size range and increases in smaller size ranges of the same particle type, unless the final particles are submicron, in which case they will not be analyzed, and the overall concentration of the particle type will decrease. Oxidation, decomposition, and vaporization reactions will also decrease particle sizes. If such reactions occur, the overall particle size may decrease without a change in particle type although new particle types may also form (such as pyrite oxidizing to iron oxide).

Increases in a given size range that are not related to decreases in larger ranges (as described above) most likely occur through condensation of gaseous species, or coalescence or agglomeration of particles. If the condensation of gaseous species occurs heterogeneously, and if the nucleus is of different composition than the condensate, particles with new compositions may be formed. However, if little interaction of the condensate with the nucleus occurs, then a particle with a larger diameter than the nucleus and with a layered composition is formed. If the particle is sectioned during preparation, then the CCSEM will assign the particle to the inorganic type that has the composition of the nucleus. If the particle is not sectioned during preparation (as may occur if the particle is associated with a bubble in the epoxy or inside a char particle), then the measured composition of the particle will be that of the coating, and the particle will be assigned to the inorganic type that has the same composition as the coating. If the condensation of gaseous species occurs through homogeneous nucleation, the particles will be predominantly submicron, although the initial particles may then coalesce or agglomerate to form larger particles.

Coalescence and agglomeration of particles will, in general, lead to particle size increases accompanied by decreases in smaller size ranges, unless the original particles were submicron, in which case the overall concentration of the particle type will appear to increase. Coalescence and agglomeration may also cause the formation of new particle types.

Finally, both decreases and increases in concentrations of particle types within a given size range may be due to statistical reasons. Because the average diameter categories vary by a factor of $10^{1/3}$, then the average areas of particles within adjacent size categories vary by a factor of $10^{2/3}$. The difference in average areas between a particle in the smallest size category and one in the largest is a factor of $(10^{2/3})^5$ or 2154. Since only a few

thousand particles were analyzed in a sample collected at a given port, a difference of a few particles in the largest size category could mean large differences in the overall concentration of the large particle type as compared to the other particle types.

Statistical variation in the numbers of quartz particles and pyrite particles analyzed in the Robinson coal and Robinson Port 1 samples appears to be the largest factor in causing the changes in concentration in the largest size range of those types between the coal and the Port 1 particulate sample. Of the 1480 particles analyzed in the Robinson coal, only 7 were pyrite particles with diameters that fell in the largest size range, yet they constituted over 20% of the inorganic particle area analyzed. Of the total 2132 particles analyzed in the different cyclone samples collected at Port 1, only 6 were quartz particles that had diameters in the largest size range, yet nearly 20% of the inorganic particle area analyzed was due to these particles. In each case, the standard deviation in the values, based on counting statistics, is approximately 40%. In addition to statistical reasons, the decrease in the concentration of pyrite in the Port 1 samples as compared to the coal may be due to fragmentation and chemical reaction to form iron oxide, pyrrhotite, or minerals classified as unknown.

TEM. The Robinson Port 1 char particles appeared to be of the same two types as those seen in the Eagle Butte sample. Figure 36 shows an example of the highly vesicular char type. As seen in the figure, the Robinson char particles of this type appeared to be more fractured than the highly vesicular Eagle Butte char particles collected at Port 1. The ash globules on the surfaces of the char particle shown in Figure 36 were high in calcium. Figure 37 is a closeup (13,500x) of a portion of the char particle shown in Figure 36 that shows several of the ash globules. Of the four largest globules that lie along a central vertical line, the top particle is calcium aluminate, the next lowest is calcium oxide, and the large globule second from the bottom has the composition of the calcium-aluminosilicate particle type.

3.10 Inorganic Composition of the Port 2 Particulate Samples

3.10.1 Eagle Butte Port 2

Elemental. By the time the particulates reach the sampling probe at Port 2, the coal has undergone 96.3% burnout. The total residence time in the refractory-lined portion of the combustor is approximately 0.2 seconds. The maximum equilibrium temperature reached by an extraneous inorganic particle by the time it reaches the sampling probe is approximately 1367°C. That temperature is reached immediately before the probe.

The inorganic elemental contents of the ASTM ashes of the cyclone-separated Eagle Butte particulates collected at Port 2 of the combustor are listed in Table 27. They are listed on a metal oxide basis. The metal oxides have been normalized to total 100% on an SO_3-free basis to make comparisons with the coal data easier. The SO_3 numbers are given on a basis normalized with the other elemental oxides. Because the filter sample was too small for separate analysis, a portion of it was mixed with the Cyclone 3 sample in an amount proportional to their weights.

Figure 36. TEM photograph (3,300x) of a highly vesicular Robinson char particle collected at Port 1.

Figure 37. TEM photograph (13,500x) of a portion of the char particle pictured in Figure 36 showing calcium-rich ash particles.

TABLE 27

INORGANIC ELEMENTAL COMPOSITION OF EAGLE BUTTE PORT 2 CYCLONE SAMPLES

Elemental Oxide	Cyclone 1 (%)	Cyclone 2 (%)	Cyclone 3+F (%)
Na_2O	1.7	3.4	5.9
MgO	5.5	8.3	7.8
Al_2O_3	14.8	20.7	18.4
SiO_2	34.5	24.5	19.0
K_2O	0.2	0.2	0.4
CaO	32.2	34.0	30.1
TiO_2	0.9	1.2	10.2
MnO	0.1	0.1	0.1
Fe_2O_3	10.0	7.6	7.2
SO_3	3.3	1.5	5.1

No significant changes from the Port 1 concentrations of Mg, Al, Si, K, Mn, and Fe oxides are seen in the various cyclone samples collected at Port 2. Na does show a slight decrease in concentration in the largest particles and a slight increase in the smallest particles. This may imply further volatilization of sodium from the char present at Port 1 followed by condensation in the smallest aerodynamic sizes. Ca shows a slight increase in the Cyclone 1 sample and a decrease in the Cyclone 3 sample collected at Port 2 over the samples collected in the same cyclones at Port 1. This may imply a slight agglomeration of high-calcium particles or a possible increase in condensation on larger particles over the amount found in the Port 1 samples. The concentration of Ti appears anomalously high in the Cyclone 3 + filter sample collected at Port 2. The reason for the increase is not known. The concentration of sulfur has significantly decreased in all of the Port 2 samples as compared to the Port 1 samples. This implies volatilization of sulfur from the char between Port 1 and Port 2 and little subsequent condensation of sulfur species. The volatilization correlates with an increase in the concentration of SO_2 in the combustor gas.

Crystalline. X-ray diffraction analysis of the Eagle Butte, Port 2, Cyclone 1 sample shows the presence of quartz as a major phase, as did the XRD of the Port 1 sample. In contrast to the Port 1 sample, the amorphous background around the quartz peak was much lower in the Port 2 sample because of the greater level of burnout in the Port 2 sample. In addition, minor phases of lime (CaO) and periclase (MgO) were evident in the Port 2 sample which were not seen in the Port 1, Cyclone 1 analysis. The higher lime peak in the Port 2, Cyclone 1 diffractogram may support the inorganic elemental analysis that showed higher levels of Ca in that sample as compared to the Port 1, Cyclone 1 sample, or may simply reflect the overall lower amorphous background signal in the Port 2 diffractogram.

The diffractogram of the Port 2, Cyclone 2 sample shows major peaks due to quartz, lime, periclase, and an Al-Fe phase that does not have a common name listed. The lime and periclase are much higher relative to the quartz peak than they are in the Port 1, Cyclone 2 diffractogram. The formation process of the Al-Fe phase is not understood.

The diffractogram of the Port 2, Cyclone 3 sample shows a strongly amorphous background with a weak lime peak. This is in contrast to the diffractogram of the Port 1, Cyclone 3 diffractogram that shows a somewhat stronger lime peak as well as a periclase peak. The reason for the reduction in the peak sizes in the diffractograms of the Cyclone 3 samples collected at Port 2 as compared to Port 1 may be due to incorporation of the lime in agglomerates, or, along with the periclase, in amorphous phases that formed due to the higher temperature and more reducing atmosphere present at Port 2.

CCSEM. The results of the CCSEM analyses of the Cyclone 1, Cyclone 2, and Cyclone 3 + filter samples collected at Port 2 during a combustion test of the Eagle Butte coal were combined to give a calculated CCSEM analysis of the bulk sample collected at Port 2. The calculated bulk data is shown in Table 28. Only those inorganic types that show area concentrations greater than 0.5% of the total inorganic particle area analyzed are presented in the table.

The CCSEM data in Table 28 shows that the overall average diameters of the inorganic particles have decreased relative to the Port 1 inorganic particles. The area of particles falling in the largest size range is dropped 20%, whereas the total area of particles in the 22-46-μm range has dropped by 30%, as compared to the particles collected at Port 1. These decreases have been made up for by an increase of 28% in the area of particles that have average diameters in the 10-22-μm size range, and smaller increases in the next two smaller size ranges. This shows that some fracturing has occurred in the inorganic particles as the level of burnout increased from 50.8% to 96.3%.

Most of the overall reduction of particle size occurred in the quartz classification. In addition, the concentration of quartz in the particulate sample has decreased by 60%. A large portion of the decrease in quartz has been made up for by an increase in the Ca-Al-silicate, Ca-silicate, and unknown categories. This shows a substantial interaction of Al, Ca, and other elements with the quartz particles. Since the level of the aluminosilicate did not drop, the aluminum to form the Ca-Al-silicate must be from another source. The chemical fractionation data for Eagle Butte shows that nearly 40% of the aluminum in the coal is associated in an acid-extractable form, possibly in organic coordination complexes. The liberation of the aluminum due to the increased burnout of the coal may be the source of the aluminum that was used in creating the Ca-Al-silicate. The source of the Ca used to create the Ca-Al-silicate and Ca-silicate is also likely to be an organically associated form since the chemical fractionation data shows that over one-third of the calcium is in ion-exchangeable form in the coal.

In addition to reacting with the quartz in the coal, the Ca also appears to be forming substantial amounts of Ca-rich particles and smaller amounts of calcite. The Ca also combined with Al to form the Ca-aluminate inorganic particle type.

TABLE 28

THE CALCULATED RELATIVE AREA PERCENTS OF THE INORGANIC PARTICLES IN THE EAGLE BUTTE, PORT 2, BULK PARTICULATE SAMPLE

Average Diameter (μm)	1.0-2.2	2.2-4.6	4.6-10	10-22	22-46	>46	Total
Quartz	0.3	1.2	1.8	14.8	7.5	4.5	30.1
Iron Oxide	0.0	0.1	0.0	0.7	2.8	1.9	5.5
Al-Silicate	0.0	0.4	0.8	3.5	4.6	0.0	9.3
Ca-Al-Silicate	0.1	1.3	1.3	4.9	2.5	0.0	10.1
Fe-Al-Silicate	0.0	0.0	0.0	0.0	1.8	0.0	1.8
K-Al-Silicate	0.0	0.0	0.1	0.2	0.0	0.0	0.3
Ankerite	0.0	0.1	0.1	0.5	0.0	0.0	0.7
Ca-Silicate	0.1	0.3	0.4	4.9	3.2	0.0	8.9
Gyp/Al-Silicate	0.0	0.1	0.0	0.0	0.0	0.0	0.1
Ca-Aluminate	0.1	0.8	0.8	0.6	0.4	0.0	2.7
Calcite	0.0	0.6	0.5	0.9	0.0	0.0	2.0
Pyrrhotite	0.0	0.0	0.0	0.0	0.0	2.8	2.8
Ca-Rich	0.4	3.0	1.9	3.8	0.4	0.0	9.5
Si-Rich	0.1	0.2	0.2	1.2	0.0	0.0	1.7
Unknown	0.6	2.6	1.7	4.0	4.2	0.0	13.1
Total	1.7	10.7	9.6	40.0	27.4	9.2	98.6

Fe also appears to be active during this stage of combustion. The pyrite that was present in the Port 1 sample is now gone, while a substantial increase in iron oxide was evident along with the formation of pyrrhotite and Fe-Al-silicate inorganic particle types. In addition, ankerite-like particles were formed through reactions between Fe, Ca, and possibly Mg.

TEM. As in the case of the Port 1 samples, two main types of char were evident in the ultrathin sections of the Port 2 samples--highly vesicular particles and higher density particles that contain much less void space. Figure 38 is a 3,300x TEM photograph of two char particles that have the highly vesicular structure. The ash particles associated with such particles tend to be large globules lightly attached to internal and external char surfaces. The association is illustrated in Figure 39, which is a 10,500x TEM photograph of the smaller vesicular char particle shown in Figure 38. In addition to the large ash globules, the char particles contain high levels of the 3×10^{-3}-μm and 3×10^{-2}-μm high-contrast inclusions that were seen in the coal. These inclusions are shown in Figure 40 which is a 82,000x TEM photograph of the char particle in Figure 39. The smallest inclusions have undergone little change as compared to the appearance of the inclusions in the coal.

The concentration of the smallest inclusions appears to be high because they scatter electrons much better than the char in which they are embedded.

Figure 38. TEM photograph (3,300x) of highly vesicular char particles collected at Port 2 during combustion testing of Eagle Butte coal.

Figure 39. TEM photograph (10,500x) of the small char particle shown in Figure 38 illustrating the relationship between the char and ash.

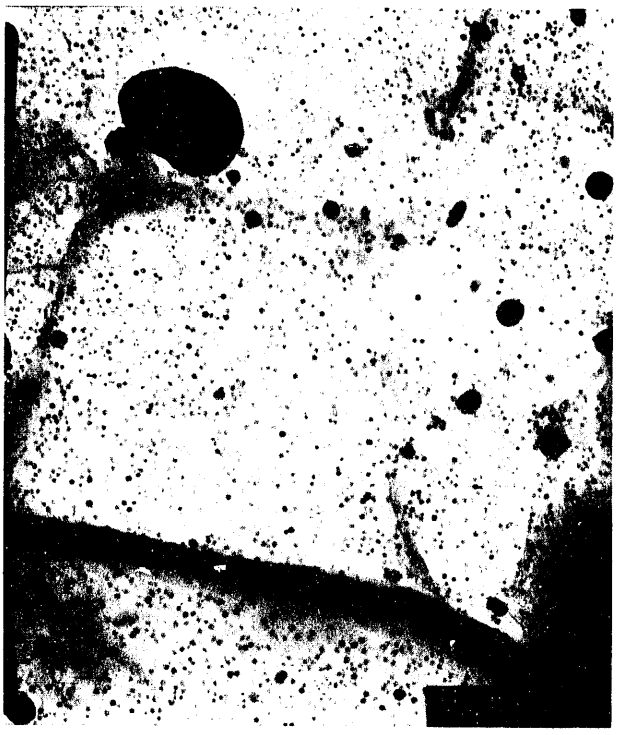

Figure 40. TEM photograph (82,000x) of the char particle shown in Figure 39, illustrating the unchanged nature of the $3x10^{-3}$-μm and $3x10^{-2}$-μm high-contrast inclusions.

In actuality, the thickness of the thin section is approximately 50 times the thickness of the smallest part. The mass concentration of each size class of particles can be calculated using Equation 21.

$$M_i/M_c = (4\pi/3)(R_i)3N_iD_i/(D_c) \qquad \text{[Eq. 21]}$$

Where: M_i = mass of inclusions
M_c = mass of bulk char
N_i = number of inclusions per unit volume of char
R_i = radius of inclusion
D_i = inclusion density
D_c = char density

In order to calculate the actual mass concentration of the small inclusions, several assumptions must be made. It is assumed that the particles have a density equal to that of quartz (2.6 g/cm^3), whereas the bulk char i.e., carbonaceous and noncarbonaceous, has a density equal to the density of coal (1.3 g/cm^3). Also, the average concentration of the particles in the char will be assumed to be equal to the concentration of particles shown in Figure 40. This is a liberal assumption, since the concentration shown in

Figure 40 is a relatively high one, and because not all char particles exhibited the small inclusions. Finally, the total volume of sample imaged in Figure 40 will be assumed to be 0.1 μm thick and composed entirely of char (and not resin). Under these assumptions, the volume of char imaged in Figure 40 is approximately 0.11 μm^3. By counting the number of particles in the photograph that belong to a given size and dividing by the volume of char imaged, the number of particles per unit volume can be calculated. In Figure 40 there are approximately 5800 of the smallest size class of particles (average diameter of approximately 3×10^{-3} μm). Using the preceding assumptions, the mass concentration of the inclusions within the char particles that carry the maximum concentrations of inclusions is calculated to be 0.15%. Assuming the concentration is the same in the coal and that the inclusions form ash in a weight ratio of 1:1, then only about 2.5% of the weight of the ASTM ash is formed by the smallest inclusions. The mass concentration of the next larger class (3×10^{-2} μm) is approximately 0.5% of the char or 8.6% of the ash.

Figure 41 shows a TEM photograph (4,900x) of the second type of char particle, the type that shows much less void space than the highly vesicular char. Like the vesicular char, the two smallest size classes of high-contrast inclusions are sometimes found in the more dense char particles. The inclusions in the higher density char collected at Port 2, however, show some coalescence which causes the distinctions between the size classes to become less pronounced. Unlike the smallest high-contrast inclusions, the large globular particles of ash that are often associated with the highly vesicular chars are absent. This may be because this type of char particle burns more slowly than the vesicular char particles. The slower burning rate means that the char surface recedes more slowly so that particles are brought together to coalesce at a slower rate. If the particles are shed at a higher rate than the coalescence rate, then larger globular ash particles will not form during combustion of such char particles. The photograph is also interesting in that it shows two physical features of the ultrathin sections. First, grooves in the section, generally running right to left and sloping upwards slightly to the left, are caused by imperfections in the knife edge, most commonly remnants of previous sections. In addition, wrinkles generally run vertically or point toward the char section. The closeness of the wrinkles gives a visual indication of the ratio of length to thickness of the ultrathin sections. Assuming a length of 0.7 mm and a thickness of 0.1 μm, the length-to-thickness ratio of the ultrathin section is approximately 7000 to 1. The length-to-thickness ratio of writing paper is approximately 4000 to 1.

3.10.2 Robinson Port 2

Elemental. By the time the particulates reached the sampling probe at Port 2, the Robinson coal had undergone 90.8% burnout. The total residence time in the refractory-lined portion of the combustor was approximately 0.2 seconds. The maximum equilibrium temperature reached by an extraneous inorganic particle by the time it reached the sampling probe was approximately 1370°C. That temperature was reached immediately before the probe.

Figure 41. TEM photograph (4,900x) of a high-density char particle collected at Port 2 during an Eagle Butte combustion test.

The inorganic elemental contents of the ASTM ashes of the cyclone-separated Robinson particulates collected at port 2 of the combustor are listed in Table 29. They are listed on a metal oxide basis and have been normalized to total 100% on an SO_3-free basis. The SO_3 numbers are given on a basis normalized with the other elemental oxides.

The concentrations of Mg, K, Ca, Ti, and Mn showed little change in distribution between the cyclone samples collected at Port 2 as compared to the samples collected at Port 1. Na, Al, and Fe showed overall decreases that are not significant. The only significant redistributions of elements among the cyclone samples were seen in the concentrations of Si and S. Si showed an increase in the largest aerodynamic diameter particles and a decrease in concentration in the smaller particles implying coalescence of inorganic particles that contain Si. This is in contrast to the Eagle Butte data that showed the opposite implication of fragmentation of Si containing particles. The large reductions in S in each of the cyclone samples collected at Port 2 as compared to those collected at Port 1 follow the trend seen in the Eagle Butte combustion tests. The reductions imply high levels of vaporization of S between 32% and 91% burnout. The decrease in S in the particulate matter is balanced by an increase in SO_2 in the combustor gas.

Crystalline. The x-ray diffractograms of each of the cyclone samples collected at Port 2 showed reduced amorphous background signals as compared to the Port 1 samples. The XRD of the Cyclone 1 sample showed only a

TABLE 29

INORGANIC ELEMENTAL COMPOSITION OF ROBINSON PORT 2 CYCLONE SAMPLES

Elemental Oxide	Cyclone 1 (%)	Cyclone 2 (%)	Cyclone 3 (%)
Na_2O (%)	2.7	5.3	9.4
MgO (%)	2.7	3.9	3.4
Al_2O_3 (%)	15.4	18.7	22.7
SiO_2 (%)	45.0	28.5	27.6
K_2O (%)	0.2	0.2	0.2
CaO (%)	17.0	23.2	21.6
TiO_2 (%)	0.6	0.5	0.5
MnO (%)	<0.1	<0.1	<0.1
Fe_2O_3 (%)	16.2	5.0	3.2
SO_3 (%)	7.5	2.0	2.8

quartz peak. As was true for the Eagle Butte Cyclone 2 samples, however, the Robinson Cyclone 2 sample showed a greater variety of crystalline phases present than either the Cyclone 1 or 3 samples. The major crystalline species present in the Cyclone 2 samples are quartz, lime, and periclase. In addition, smaller peaks due to magnetite (Fe_3O_4) are present. The presence of magnetite in the Cyclone 2 sample and not in the Cyclone 1 sample supports the hypothesis that the pyrite originally present in the coal fragmented on combustion to much smaller sizes, many of which may had submicron diameters. The magnetite peak may not have been obvious in the Port 1 diffractograms because of the large amorphous backgrounds present in those diffractograms. The diffractogram of the Cyclone 3 sample shows a large amorphous background signal with small peaks due to periclase.

CCSEM. The calculated inorganic particle-size distribution of the bulk particulate sample collected at Port 2 during combustion testing of the Robinson coal is shown in Table 30. The values for the table of bulk data were found by multiplying the values in the separate cyclone tables by a fraction equal to the fraction of the total ASTM ash that was collected in that cyclone, then adding the prorated values. Only those inorganic particle types that showed total concentrations of at least 0.5% of the total inorganic particle area are shown.

The overall changes in inorganic particle-size distribution between the Port 1 and Port 2 particulate samples follow the trend shown between the coal and Port 1 samples in that the area fraction of the 10- to 46-μm average diameter inorganic particles has decreased. The largest reductions in that

TABLE 30

THE CALCULATED RELATIVE AREA PERCENTS OF THE INORGANIC PARTICLES IN THE ROBINSON, PORT 2 PARTICULATE SAMPLE

Average Diameter (μm)	1.0-2.2	2.2-4.6	4.6-10	10-22	22-46	>46	Total
Quartz	0.6	2.1	1.1	3.6	7.1	15.6	30.1
Iron Oxide	0.0	0.2	0.1	0.6	1.8	0.0	2.7
Al-Silicate	0.7	1.7	0.9	1.9	1.9	1.9	8.9
Ca-Al-Silicate	1.1	3.0	1.6	2.4	2.4	0.6	11.1
K-Al-Silicate	0.0	0.1	0.0	0.0	0.2	0.0	0.3
Ankerite	0.0	0.3	0.0	0.1	0.0	2.5	2.9
Barite	0.0	0.1	0.0	0.0	0.0	1.2	1.3
Ca-Silicate	0.2	0.8	0.5	1.2	1.1	4.4	8.2
Ca-Aluminate	0.1	0.6	0.4	0.2	0.2	1.2	2.8
Calcite	0.0	0.2	0.1	0.4	0.0	0.0	0.6
Pyrrhotite	0.0	0.0	0.0	0.1	0.3	4.4	4.8
Ca-Rich	0.4	1.7	1.4	0.7	1.1	1.2	6.5
Si-Rich	0.0	0.1	0.0	0.2	0.3	0.0	0.6
Unknown	0.6	1.4	0.8	0.9	1.2	13.2	18.0
Total	3.8	12.2	7.0	12.2	17.6	46.3	99.0

range occur in the quartz and aluminosilicate particle types. Some of the reduction is compensated for by an increase in the 2.2 to 4.6 μm range for the calcium aluminosilicate particle type, demonstrating possible fragmenting of aluminosilicate grains in conjunction with coalescence with high-Ca particles. The largest increase in area fraction occurs in the >46-μm range, however. The largest increases in that size range occur in the calcium silicate, pyrrhotite, and unknown particle types. The increase in the calcium silicate and unknown categories indicates coalescence of smaller silicate grains along with coalescence of calcium rich and other particles. The increase in pyrrhotite indicates partial oxidation of pyrite over this stage of combustion. The large size of the pyrrhotite grains indicates either coalescence of pyrrhotite grains formed from smaller pyrite particles, or may indicate that the values for the concentration of pyrite in the Port 1 sample for this size range were anomalously low, possibly due to poor counting statistics.

In addition to changes in the concentrations of phases that were present in the Port 1 sample, calcium aluminate and ankerite formed during this stage of combustion. Since the calcium was originally present in the coal in a predominantly organic association, the large sizes of the ankerite and calcium aluminate particles suggests either rapid coalescence of small particles of those species, or that they are present as condensed coatings on larger nucleate particles and that they were not sectioned during sample preparation.

The Robinson Port 2 char and ash particles observed in the TEM differed little from the particles seen in the Port 1 samples with two qualitative exceptions. The first is that the elemental compositions of the ash particles showed greater complexity than the ash particles seen in the Port 1 sample. Second, the concentration of calcium aluminate particles in the submicron size range appears much higher than its concentration in the supermicron size range as determined in the CCSEM analysis.

3.11 Inorganic Composition of the Port 10 Particulate Samples

3.11.1 Eagle Butte Port 10

Elemental. By the time the particulates reach the sampling probe at Port 10, the coal has undergone 99.8% burnout. The total residence time in the refractory-lined portion of the combustor is approximately 2.4 seconds. The equilibrium temperature of an extraneous inorganic particle at Port 10 is approximately 1055°C.

The inorganic elemental contents of the ASTM ashes of the cyclone-separated Eagle Butte particulates collected at Port 10 of the combustor are listed in Table 31. They are listed on a metal oxide basis. The metal oxides have been normalized to total 100% on an SO_3-free basis. The SO_3 numbers are given on a basis normalized with the other elemental oxides. Because the filter sample was too small for separate analysis, a portion of it was mixed with the Cyclone 3 sample in an amount proportional to their weights.

The distribution of the elements among the cyclone samples collected at Port 10 shows little change from the distribution among the samples collected at Port 2, with the exception of Ca, Fe, and S. For each of those elements, small decreases in their concentrations in the Cyclone 1 sample are accompanied by increases in the Cyclone 2 and/or Cyclone 3 samples. The changes in concentration of Ca and Fe imply either volatilization from the larger particles followed by recondensation in the smaller particles, or some fracturing of the inorganic particles that contain Ca or Fe. The increase in S in the smaller aerodynamic size particles is caused by either fracturing of inorganic particles that contain S, or increased S capture by the smallest size fraction. The latter hypothesis is supported by the fact that the concentration of SO_2 in the combustor gas is lower at Port 10 than at Port 2.

Crystalline. The XRD analysis of the Cyclone 1 sample shows no change from the Cyclone 1 sample collected at Port 2; i.e., only a major phase of quartz and minor phases of lime and periclase are present. The XRD of the Cyclone 2 sample shows major phases of lime and periclase as did the Port 2 sample. In contrast to the Port 2 sample, the height of the quartz peak is reduced, no Al-Fe phase is shown, and peaks corresponding to a crystal phase termed "sulfurous aluminum clinker" are evident. The inorganic elemental oxide composition of sulfurous aluminum clinker is listed as 43% CaO, 22% Al_2O_3, 22% SO_3, and minor amounts of SiO_2 and other oxides. The XRD of the Cyclone 3 + filter samples shows a strong periclase peak along with weak lime and anhydride ($CaSO_4$) peaks. The presence of these crystal phases is in contrast to the presence of only a weak lime peak in the Cyclone 3 sample collected at Port 2. The formation of anhydride in the Port 10 sample

TABLE 31

INORGANIC ELEMENTAL COMPOSITION OF EAGLE BUTTE PORT 10 CYCLONE SAMPLES

Elemental Oxide	Cyclone 1 (%)	Cyclone 2 (%)	Cyclone 3+F (%)
Na_2O	2.0	3.3	4.1
MgO	6.7	9.0	9.4
Al_2O_3	16.9	20.1	20.2
SiO_2	36.7	20.3	17.0
K_2O	0.2	0.2	0.3
CaO	28.4	38.0	38.4
TiO_2	1.9	1.2	1.1
MnO	<0.1	0.1	0.1
Fe_2O_3	7.8	7.8	9.3
SO_3	2.2	6.2	12.3

supports the hypothesis of increased sulfur capture in the small aerodynamic size particles in the Port 10 samples that was indicated by the increased S content of the Cyclone 2 and 3 samples.

CCSEM. The results of the CCSEM analyses of the Cyclone 1, Cyclone 2, and Cyclone 3 + filter samples collected at Port 10 during a combustion test of the Eagle Butte coal were combined to give a calculated CCSEM analysis of the bulk sample collected at Port 10. The calculated bulk data is shown in Table 32. Only those inorganic types that show area concentrations greater than 0.5% of the total inorganic particle area analyzed are presented in the table.

A comparison of the CCSEM data for the Port 2 and Port 10 samples shows a reduction in the total area of particles found in the largest two average diameter categories with the greatest reduction in the >46-μm range. Most of the reduction in the area percent in the >46-μm range was due to loss of quartz and pyrrhotite. The loss may have been caused by fracturing due to thermal stresses or, in the case of pyrrhotite, stresses associated with oxidation. The decrease in the largest two ranges was accompanied by an increase in total particle area found in the 10-22-μm size range. A similar shifting in average diameters was seen in a comparison between the Port 1 and Port 2 samples.

Five particle types showed reductions in concentration as the particles were carried from Port 2 to Port 10. The largest reduction occurred in the concentration of quartz, which showed reductions in concentration in all size categories. Other reductions were seen in the concentrations of iron oxide,

TABLE 32

THE CALCULATED RELATIVE AREA PERCENTS OF THE INORGANIC PARTICLES IN THE EAGLE BUTTE, PORT 10, BULK PARTICULATE SAMPLE

Average Diameter (μm)	1.0-2.2	2.2-4.6	4.6-10	10-22	22-46	>46	Total
Quartz	0.1	0.3	0.6	11.6	6.0	1.4	20.2
Iron Oxide	0.0	0.0	0.0	0.9	3.1	0.0	4.0
Al-Silicate	0.0	0.1	0.5	3.1	1.6	0.0	5.4
Ca-Al-Silicate	0.3	1.2	0.8	6.8	3.2	1.4	13.8
K-Al-Silicate	0.0	0.0	0.1	0.4	0.0	0.0	0.5
Ankerite	0.0	0.0	0.0	0.6	0.9	0.0	1.5
Gypsum	0.0	0.1	0.0	0.0	0.0	0.0	0.2
Ca-Silicate	0.1	0.2	0.4	6.6	4.2	0.0	11.5
Gyp/Al-Silicate	0.2	0.8	0.3	0.3	0.0	0.0	1.6
Ca-Aluminate	0.1	0.6	0.5	3.2	0.3	0.0	4.7
Calcite	0.0	0.5	0.5	1.6	0.0	0.0	2.6
Dolomite	0.0	0.0	0.1	0.4	0.0	0.0	0.5
Ca-Rich	0.7	2.8	2.3	7.5	3.1	0.0	16.3
Si-Rich	0.0	0.1	0.0	1.1	0.3	0.0	1.7
Unknown	1.0	3.0	1.9	6.4	3.0	0.0	15.3
Total	2.6	10.0	8.0	50.6	25.8	2.9	99.8

aluminosilicate, Fe Al-silicate, and pyrrhotite. In contrast, ten particle types showed increases in concentration between Port 2 and Port 10. The largest total increases occurred in the categories of Ca-Al-silicate, Ca-silicate, Ca-aluminate, and Ca-rich. These increases occurred predominantly in the 10-22-μm and 22-46-μm size categories, the same size ranges that showed reductions in quartz and aluminosilicate. This implies that Ca is in an active state between the two ports and reacts with existing quartz and aluminosilicate particles to form Ca-silicates, Ca-Al-silicates, and Ca-rich particles.

The fate of Fe during this period is not clear. The categories of iron oxide, Fe-Al-silicate, and pyrrhotite all showed reductions between Port 2 and Port 10. However, the only inorganic type that explicitly contains Fe and that showed an increase during this time is ankerite. The increase in ankerite is not enough to make up for the decreases in the other Fe-containing species. Therefore the decreases are either due to fragmentation resulting in submicron particles, or, more likely, to statistical variations related to the low numbers of iron-containing particles that were detected.

TEM. Although uncommon, some char particles were still evident in the Port 10 samples. Only the more dense char particles were seen, however, indicating that the more vesicular char particles had burned out. Figure 42 is a TEM photograph (10,500x) of the edge of such a char particle. Although

Figure 42. TEM photograph (10,500x) of the edge of a char particle collected at Port 10 during an Eagle Butte combustion test.

the contrast of the carbonaceous portion is low, the edge and a large pore opening can be seen implicitly by the outline of the small, high-contrast particles. Figure 43 is a TEM photograph (10,500x) of another area of the same char particle that shows how the small, high-contrast inclusions have melted. In some instances the particles have coalesced to form particles with diameters in the 0.1-μm range. In other cases, the melted particles appear to have flowed through pores within the char. The longer chain of flow regions that runs left to right across the photograph contains mostly Fe. The large particle at the right edge of Figure 43 contains high concentrations of Si and Al, and smaller amounts of Ni, Cr, and Fe (possibly stainless steel). As was the case with the more dense char particles collected at Port 2, no large globules of ash are seen at the surface of this type of char.

3.11.2 Robinson Port 10

Elemental. By the time the particulates reached the sampling probe at Port 10, the Robinson coal had undergone >99.9% burnout. The total residence time in the refractory-lined portion of the combustor was approximately 2.4 seconds. The equilibrium temperature of an extraneous inorganic particle at the position of the sampling probe was approximately 1140°C.

The inorganic elemental contents of the ASTM ashes of the cyclone-separated Robinson particulates collected at Port 2 of the combustor are listed in Table 33. They are listed as metal oxides and have been normalized to total 100% on an SO_3-free basis. The SO_3 numbers are given on a basis normalized with the other elemental oxides.

Figure 43. TEM photograph (10,500x) of a frozen flow of molten ash within pores in an Eagle Butte char particle collected at Port 10.

TABLE 33

INORGANIC ELEMENTAL COMPOSITION OF ROBINSON PORT 10 CYCLONE SAMPLES

Elemental Oxide	Cyclone 1 (%)	2 (%)	3 (%)
Na_2O (%)	4.0	8.8	10.0
MgO (%)	3.0	4.1	3.6
Al_2O_3 (%)	16.2	23.4	25.5
SiO_2 (%)	41.1	31.5	31.5
K_2O (%)	0.2	0.2	0.2
CaO (%)	17.0	23.2	21.6
TiO_2 (%)	0.6	0.5	0.4
MnO (%)	<0.1	<0.1	<0.1
Fe_2O_3 (%)	10.9	4.0	3.0
SO_3 (%)	1.7	3.8	4.4

The only important change in the distribution of the elements among the different cyclone samples between the Port 2 and Port 10 particulate samples is the reduction of sulfur in the Cyclone 1 sample and the increase of sulfur in the Cyclone 2 and 3 samples. The decrease in the Port 1 cyclone most likely occurred because of the loss of organically associated sulfur during burnout. The increase in sulfur in the Cyclone 2 and 3 samples indicates sulfur capture by the inorganic particles with the smallest aerodynamic diameters, probably because by weight those particles have larger surface areas than the larger particles. This hypothesis is supported by the fact that the SO_2 concentration increases to a maximum just below Port 2, the level at which burnout should be essentially complete. The SO_2 concentration then decreases from that point downward, implying increased sulfur capture with time. A small change in the distribution of Si among the cyclone samples was also noted. The small decrease in the Cyclone 1 sample and increases in the Cyclone 2 samples may not be significant, however, as the changes barely meet the 10% change criteria for significance. Although the concentrations of other elements do change between Port 2 and Port 10, the changes tend to be "one-way," i.e., increasing or decreasing for each cyclone sample. If it is assumed that the metallic elements are in a condensed form as the sample stream enters the multicyclone system, then one-way changes cannot take place while still conserving mass.

In all, Na, Mg, Al, and Ca show slight increases in concentration in each cyclone sample. Ti, K, and Mn show no significant change. However, Fe shows a significant decrease in concentration in each cyclone sample. It is believed that the changes in Fe content of the samples collected at each sampling position are due to varying amounts of iron-containing contaminants, principally rust from the barrel, between runs. The overall decrease in Fe content in the Port 10 samples causes the general slight increase in the concentrations of the other elements.

Crystalline. The x-ray diffractograms of the Port 10 samples are considerably more complex than the diffractograms of the Port 2 samples. The diffractogram of the Cyclone 1 sample shows a strong quartz peak, as did the Port 2, Cyclone 1 diffractogram. In addition to quartz, the Port 10, Cyclone 1 diffractogram shows weaker peaks due to lime, periclase, and magnesioferrite ($MgFe_2O_4$). The presence of the lime and periclase peaks in the Port 10, Cyclone 1 sample, but not in the Port 2, Cyclone 1 sample indicates agglomeration or coalescence of smaller periclase and lime particles between Ports 2 and 10.

The Cyclone 2 diffractogram shows strong peaks due to periclase and high carnegeite, and smaller peaks due to hematite. The lack of quartz or lime peaks that were seen in the Port 2, Cyclone 2 diffractogram implies that particles of those types and of the size that would have been captured in Cyclone 2 have either coalesced or agglomerated with other particles, or have undergone reactions to create new crystalline or amorphous phases. One of the new crystalline phases present in the Port 2 sample is high carnegeite. Since high carnegeite normally converts to the low form at 690°C, its presence shows that particle quenching in the sampling probe is rapid. The appearance of hematite and the disappearance of magnetite from the Cyclone two sample implies oxidation of the magnetite during the passage of the particles from Port 2 to Port 10.

The diffractogram of the Cyclone 3 sample is similar to the diffractogram of the Cyclone 2 sample, with the exception that magnetite may possibly be present rather than hematite (the signal to noise ratio for the peaks is small).

CCSEM. The calculated inorganic particle-size distribution of the bulk particulate sample collected at Port 10 during combustion testing of the Robinson coal is shown in Table 34. The values for the table of bulk data were found by multiplying the values in the separate cyclone tables by a fraction equal to the fraction of the total ASTM ash collected in that cyclone, then adding the prorated values. Only those inorganic particle types that showed total concentrations of at least 0.5% of the total inorganic particle area are shown.

As burnout progresses from 90% to 100% between Ports 2 and 10, the fraction of inorganic particles that have average diameters of >46 μm decreased by 75%, with the decrease being taken up as increases in the 10-22-μm and 22-46-μm size ranges. The largest decreases in the >46-μm range occurred in the quartz, pyrrhotite, and unknown categories. The decrease in pyrrhotite appears to be largely balanced by increases in iron oxide in the 10 to >46-μm average diameter size ranges, implying oxidation and some fragmentation of the pyrrhotite.

Two other particle types showing increases in the 10 to 46-μm categories are the quartz and unknown inorganic particle types showing possible fragmentation of the >46-μm particles of these types. In addition, both calcium-aluminosilicate and aluminosilicate particle types showed increases. An explanation of these two increases is difficult since an increase in calcium-aluminosilicate is usually accompanied by a decrease in aluminosilicate, implying interaction of the originally organically associated Ca with aluminosilicate particles. However, since the concentration of aluminosilicate particles also seems to have increased, this explanation is not valid or at least is incomplete. A possible explanation for the increase in aluminosilicate may be seen in the comparison of the Port 1 and Port 2 CCSEM data in which a large decrease in the concentration in the aluminosilicate particle type from Port 1 to Port 2 is seen. The decrease may have been caused by disaggregation of the platelets that make up the clay "particle" during the possibly explosive vaporization of the water associated with the clay, thereby producing large numbers of submicron clay particles. As the residence time in the combustor increases, the aluminosilicate particles may undergo coalescence to form larger particles that are again picked up by the CCSEM in longer residence time samples. Unfortunately, this scenario is not supported by the elemental analyses of the cyclone samples which show little change in the Al contents of the Cyclone 1 sample between Ports 2 and 10. Another possibility may be that the CCSEM was erroneous in its measurement of the concentration of aluminosilicate particles. At any rate, an explanation of the increase in aluminosilicate particles in the Port 10 sample is not clear at this time.

TEM. The Robinson Port 10 ultrathin sections were contaminated with ubiquitous 20 to 50-nanometer NaCl crystallites that appeared to have formed during vacuum drying of the ethylene glycol from the slot grids. The source of the NaCl is not clear. The NaCl may have been dissolved from the

TABLE 34

THE CALCULATED RELATIVE AREA PERCENTS OF THE INORGANIC PARTICLES IN THE ROBINSON, PORT 10 PARTICULATE SAMPLE

Average Diameter (μm)	1.0-2.2	2.2-4.6	4.6-10	10-22	22-46	>46	Total
Quartz	0.1	0.1	0.4	6.3	9.0	2.7	18.6
Iron Oxide	0.0	0.1	0.1	1.8	2.7	1.5	6.2
Al-Silicate	0.1	0.3	0.3	4.3	5.7	3.3	14.0
Ca-Al-Silicate	0.5	2.4	1.9	6.9	7.3	0.0	19.0
K-Al-Silicate	0.0	0.0	0.0	0.3	0.3	0.0	0.6
Ankerite	0.0	0.3	0.3	0.4	0.0	0.6	1.7
Ca-Silicate	0.0	0.4	0.3	3.6	2.8	2.5	9.6
Gyp/Al-Silicate	0.1	0.9	0.0	0.2	0.0	0.0	1.2
Ca-Aluminate	0.0	0.1	0.2	1.1	0.6	0.0	2.0
Calcite	0.0	0.4	0.6	0.2	0.9	0.0	2.1
Ca-Rich	0.3	1.6	1.6	2.1	2.1	0.0	7.7
Si-Rich	0.0	0.0	0.3	0.5	0.6	0.0	1.4
Unknown	1.0	3.5	2.6	4.8	1.1	0.7	13.7
TOTAL	2.2	10.0	8.7	32.6	33.1	11.4	98.0

particulate sample, or may have originated from an environmental source. The crystals were pervasive enough to prevent drawing conclusions about the character of the submicron inorganic particles in the Port 10 sample.

3.12 Conclusions - Similarities in the Composition and Behavior of Both Eagle Butte and Robinson Coals

Although many different reactions were seen during the combustion of each of the Eagle Butte and Robinson coals, the observations and conclusions reported in this section apply to both coals and, therefore, may indicate reactions that will occur in other western U.S. low-rank coals during p.c. combustion. It must be remembered before extrapolating the following results to other combustion conditions that the combustion system used in this study involved a premixed, nonrecirculating flame that had a maximum gas temperature 100-300°C lower than that in a typical boiler flame.

3.12.1 Earlier Stages of Combustion - Coal to 0.07 Seconds

Within the first 0.06 seconds of entering the combustor (Port 1), proximate analyses showed levels of 51% burnout for Eagle Butte and 32% burnout for Robinson. Equilibrium particle temperatures for nonreacting particles at this stage were calculated to be 1220°C in the Eagle Butte tests and 1210°C in the Robinson tests. The volatile matter and fixed carbon contents of both coals decreased in the early stages of combustion with the volatile matter content decreasing by a slightly greater relative amount than the fixed carbon

content. The smaller size fractions showed higher ash concentrations than the larger size fractions. Soxhlet extractions proved that no significant levels of tar had condensed on the particulate samples to skew the proximate results. TEM observations of ultrathin sections of char particles showed that two main types of char had formed. One type was highly vesicular and had ash globules associated with inner and outer char surfaces. The other type was much less vesicular and had little ash associated with char surfaces, even though high levels of inorganic matter were seen within the char matrix. The lack of ash associated with the surfaces of the high-density char particles indicates that the ash was shed at approximately the same rate at which it was exposed at the surface of the char particles. The origin of the two types of char particles is not known, but is most likely due to maceral differences and not inorganic content differences as similar inorganic particles were seen within the matrix of each type of char particle.

Inorganic analyses showed that Na, Mg, and Ca decreased in concentration in larger (Cyclone 1) char particles and increased in concentration in smaller (Cyclone 2 and Cyclone 3) particles within the first 0.07 seconds. The majority of each of those elements is present in the coal as salts of organic acids. The redistribution indicates rapid volatilization and condensation in the small particle sizes, possibly upon quenching in the sample probe. Sulfur showed no reduction or redistribution among the different sizes, indicating that it was not significantly released from the coal at the same time as the Na, Mg, and Ca. XRD showed only the formation of alkaline earth oxides and no interaction among existing mineral grains during this stage of combustion. CCSEM showed no significant changes in the mineral matter in the Eagle Butte sample. Some pyrite fragmentation and quartz growth was evident in the Robinson sample, but the changes may be only apparent as the counting statistics for those observations were poor. The CCSEM data also indicated formation of low levels of calcium-containing phases in the Robinson samples. TEM observations showed the presence of high-contrast inclusions with circular cross sections that belong to similar size categories in each of the coals. The size classes for the Eagle Butte coal and chars were approximately 0.003 μm, 0.03 μm, and greater than 0.06 μm. Calculations show that the smallest inclusions could make up at most 2.5% of the ASTM ash of the Eagle Butte coal whereas the middle-sized inclusions could make up at most 8.6%. The actual values are believed to be closer to one-quarter of these values. The Robinson coal and char sample inclusions are approximately 30% larger and with more size variation within a class. The inclusions are believed to be inorganic, even though the compositions of the particles in the two smallest size classes could not be clearly distinguished due to interference from organically associated elements in the coals and chars. The appearance of the inclusions did not change during the early stages of combustion.

3.12.2 Later Stages of Combustion - 0.07 to 2.4 Seconds

As the level of burnout increased, the aerodynamic diameter of the particles continually shifted from greater than 13 μm to between 0.7 and 13 μm. The relative amounts of sample collected on the filter (less than 0.7 μm aerodynamic diameter) did not change by more than 1 actual percent between any two sampling positions. However, as combustion progressed, the relative

concentrations of particles in the less than 0.7-μm range first increased and then decreased. The residence time of the particles collected at Port 2 was approximately 0.2 seconds, while those collected at Port 10 had been in the combustor for approximately 2.4 seconds. Equilibrium particle temperatures for nonreacting particles peaked at 1310°C for Eagle Butte and 1370°C for Robinson at Port 2. From Port 2 to Port 10, the temperatures decreased linearly to 1055°C and 1140°C, respectively. Proximate analyses showed levels of 96% burnout for Eagle Butte and 90% burnout for Robinson at Port 2, and greater than 99.8% burnout for each at Port 10. The proximate analyses also indicated the formation of inorganic suboxides in the smallest particles collected at Port 2. The concentrations of the suboxides were high enough to mask the presence of some or all of the fixed carbon in the Cyclone 2 and 3 samples.

The proximate analyses of the Port 10 samples showed a percentage of volatile matter remaining in the samples. The long residence times of the particles in the combustor up to the Port 10 sampling point coupled with the high temperatures experienced by the particles indicate that the volatile proximate test takes place at a lower temperature than the gas temperature at the Port 10 sampling point, indicating that the volatile matter may have formed after the particulates were taken from the combustor, possibly in the cyclones as CO_2 or SO_x in the cooled combustor gas passed over them. Calcium carbonate, sodium pyrosulfate, and sodium sulfite are a few compounds that may have formed that decompose at temperatures below the temperature at which volatile matter content is determined (950°C).

TEM observations of ultrathin sections of the Port 2 chars show little change from the Port 1 char samples. Only the high-density char particles were present in the samples collected at Port 10, showing that the more dense char particles were less reactive than the highly vesicular char particles.

Bulk inorganic analysis showed that large amounts of sulfur were lost from all size ranges between Port 1 and Port 2. Some of the sulfur was recaptured by the time the particulates reached Port 10, especially in the smaller size particles. The release and recapture was supported by gas and XRD analyses. No other redistributions of elements among the different size classes were measured during the later stages of combustion. The element redistribution data suggest that the alkali metal and alkaline earth elements are not in the gas phase at the same time as sulfur species.

XRD showed the formation of considerably more complex phases in both coals in the later stages of combustion. In addition, growth in the size of alkaline earth oxide particles was indicated by the appearance of peaks in the larger cyclone samples.

CCSEM indicated the fragmentation of the largest inorganic particles to form more particles in the 10-46-μm range, although absolute determinations of the degree of particle-size change were hampered by poor counting statistics for the larger particle-size data. Formation of new calcium-containing species in the latter stages of char combustion was measured. Both coals exhibited the formation of calcium aluminosilicate, calcium silicate, calcium

aluminate, and calcium-rich particle types. The calcium-containing species formed through the coalescence of calcium oxide particles with other inorganic particles on char surfaces. The oxidation of pyrite to the pyrrhotite particle type occurred in both coals between Port 1 and Port 2. Further oxidation to the iron oxide particle type occurred between Port 2 and Port 3.

TEM observations of ultrathin sections of chars showed no changes in the appearance of the 0.003 or 0.03-μm inclusions between Port 1 and Port 2. However, the formation of new calcium species was seen in the larger sizes. The proportion of calcium aluminate-type submicron particles was relatively high compared to its concentration measured by CCSEM. By the time the Eagle Butte char particles had reached Port 10, coalescence of the smallest inclusions had occurred to the extent that distinct size classes were no longer evident. In addition, slag appeared to have formed from coalesced ash particles that appeared to flow within pores in the char. The Robinson Port 10 TEM samples were contaminated with high concentrations of NaCl that appeared to have dissolved in the microtome boat fluid and then precipitated as the fluid was dried. The crystals were so ubiquitous that no in-depth TEM observations of the Robinson Port 10 samples were carried out. The source of the NaCl is not known, but may have been from the ash itself or may have been a contaminant.

3.13 Interpretation of Fly Ash Particle-Size and Composition Evolution for Beulah and Upper Freeport

3.13.1 Introduction

Particle-size distributions of minerals and amorphous phases were determined using CCSEM for CIT test coals and chars, including the Beulah lignite and Upper Freeport. Data produced on the chars were obtained by analyzing whole grain mounts of the chars on double-stick tape. The results were checked using cross-sectioned char mounts producing the same overall particle-size distribution number percent results. The number of mineral particles in each of the following size categories was determined: <1.2, 1.2-2.1, 2.1-4.4, 4.4-8.0, 8.0-11.0, and >11.0 microns. This information provides a basis for understanding the fragmentation or coalescence of minerals during combustion of these test coals.

More detailed analysis was made of the Beulah and Upper Freeport coal, char, and fly ash inorganics by observing weight percent concentrations of inorganics in different size categories. Total inorganic particles were plotted versus size using a geometric size distribution in order to observe the overall distribution particles greater than 11 microns. In addition, weight percent concentrations of selected minerals that were being transformed or produced with time during the combustion process were plotted as a function of size. In effect, this gives a time-resolved look at inorganic transformations. Using this information, the interaction of different minerals and inorganics was described.

The end result of this approach to studying fly ash is that particle size and composition evolution with time can be observed through time, and this information gives helpful input into models which attempt to predict fly ash size and composition.

3.13.1.1 Beulah

The whole grain mount analysis of Beulah char phases revealed that greater quantities of larger-sized particles were formed during char formation as compared to the original mineral size distribution (Figure 44). This is apparent evidence for coalescence of smaller inorganic particles to form larger ones. Analysis of the cross-sectioned chars revealed similar number percent distributions of Beulah fly ash particles, indicating coalescence with time (Figure 45). Comparison of cross-sectioned coal minerals, ash particles in 0.5 and 0.8-second char ash particles, and 100% carbon burnout fly ash particles was performed on a weight percent basis as shown in Figure 46. Residence time for the fly ash was about 1.5 seconds. Coalescence is evident for the inorganics, with the final fly ash showing the most mass in the >10-μm fraction and the least amount of material in the <10-μm range.

Quartz was reduced in quantity with time, showing an almost even degradation with time (Figure 47). The reduction is primarily the result of reaction, with vapor phase Na and Ca coming out of the organic bonding sites in the coal matrix. Calcium silicate, which was nonexistent in the coal, comprised nearly 4% of the ash at 0.8 seconds. Sodium silicates appear to form only as a skin on quartz particles. Although no CCSEM category currently exists to classify sodium silicate, examination of the data found that approximately 1% of the quartz grains contained 2% or more sodium. Previous work revealed the presence of Na-rich sulfates and silicates mainly on the surface layers of Beulah chars and fly ash (3,4).

Aluminosilicates derived from clay minerals such as kaolinite and halloysite reacted pervasively with organically bound Na and Ca. The most obvious evidence for this conclusion is the production of calcium aluminosilicate with time, as shown in Figure 48. Reaction of CaO with aluminosilicates appears to be especially promulgated among the smaller-sized clay grains (<10 μm) which are more intimately associated with the organic matrix and, though small, comprise a large reactive surface area. Figure 48 reveals that calcium aluminosilicates, which are virtually nonexistent in the coal, are more abundant in the smaller size ranges of char during early combustion, but with time coalesce to form particles that are mostly greater than 10 microns in average diameter. A plot of the aluminosilicate distribution with time, given in Figure 49, shows that initially the clays are abundant in the smaller size ranges, but, upon combustion, the concentrations in the smaller size ranges decrease dramatically with an increase in larger-sized grains. This is evidence again for the interaction between organically bound Ca and aluminosilicate to transform mineral aluminosilicates, such as kaolinite, to calcium aluminosilicates during combustion.

Reaction of sodium with clay minerals is also evident from the CCSEM data. Figure 50 illustrates that Na may have a similar reactivity with the clays as Ca does because they have concentrations somewhat proportional. The 0.8-second char contained about 5% Na-bearing aluminosilicates, the Na being at least 3% or more of the particle, based on CCSEM EDS levels. Approximately 2% of the 0.8-second char also consisted of Na-bearing calcium aluminosilicates, again with the sodium being at least 3% of the EDS particle composition.

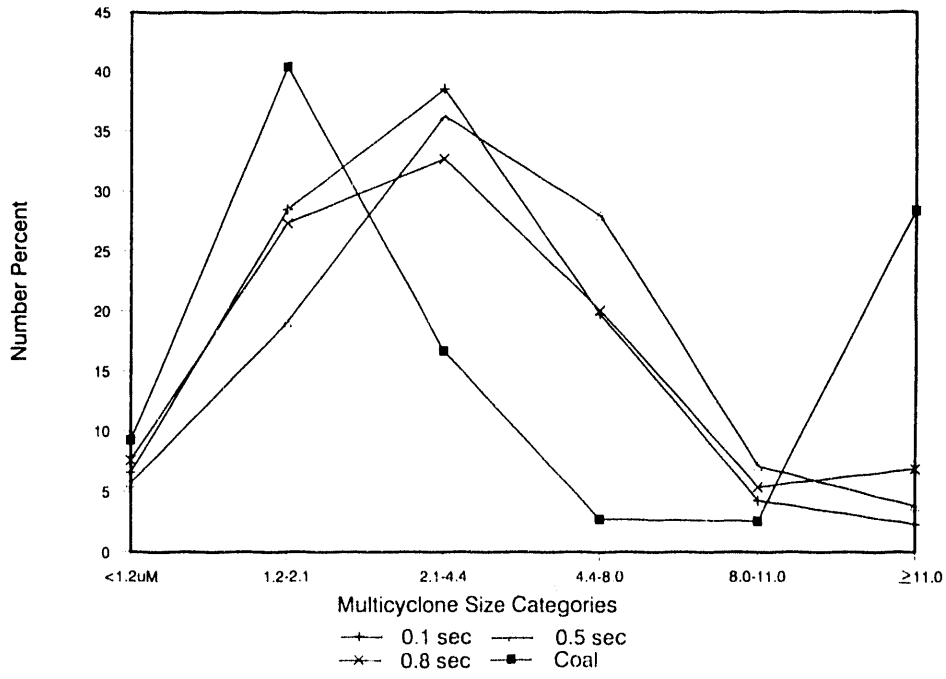

Figure 44. Whole-grain mount particle-size distribution of Beulah coal and char phases.

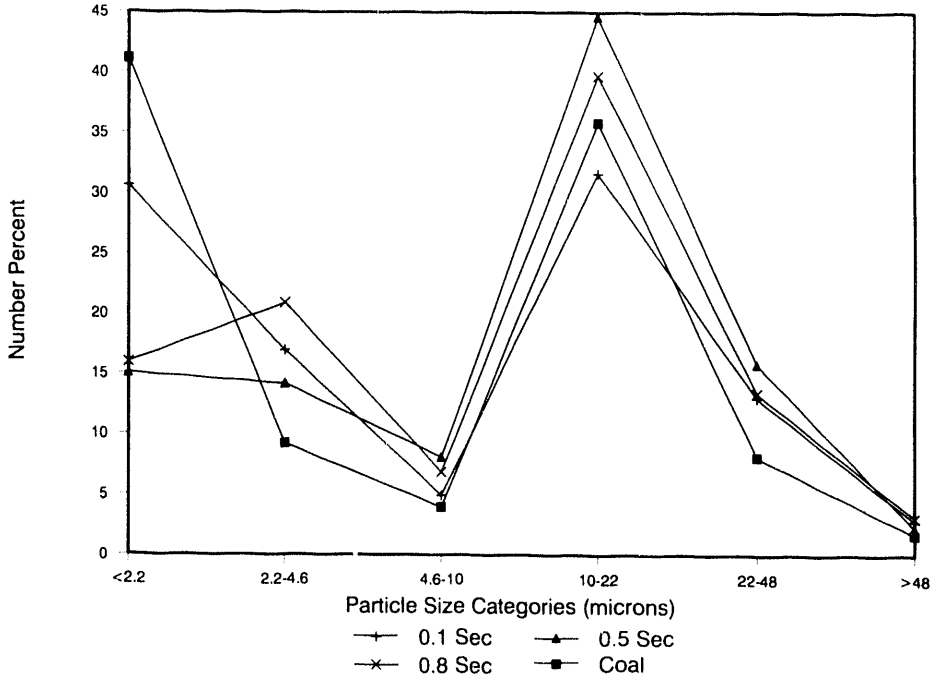

Figure 45. Cross-section particle-size distribution of Beulah coal and char phases.

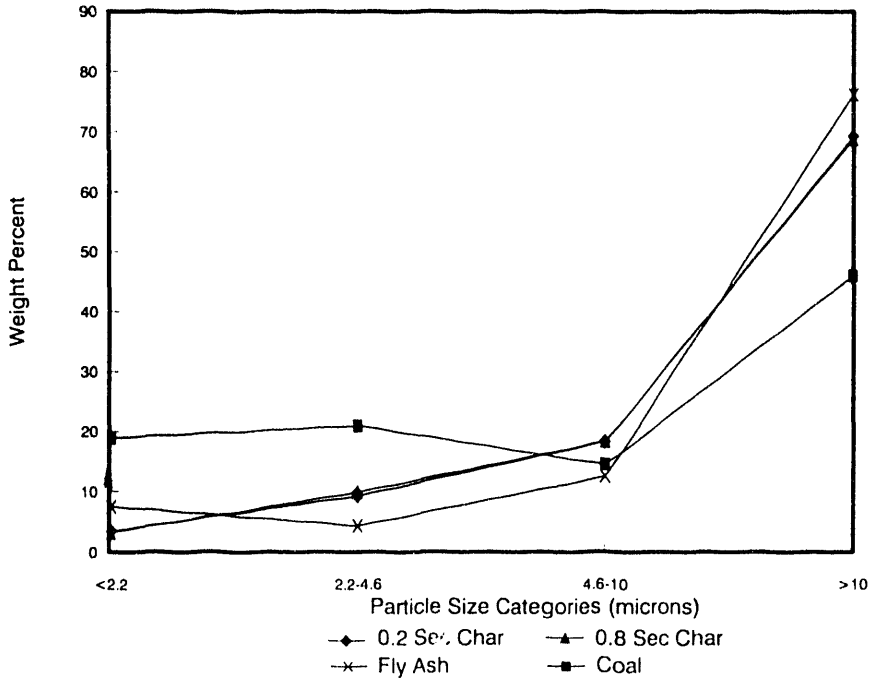

Figure 46. Cross-section particle-size distribution of Beulah coal minerals, char phases, and fly ash.

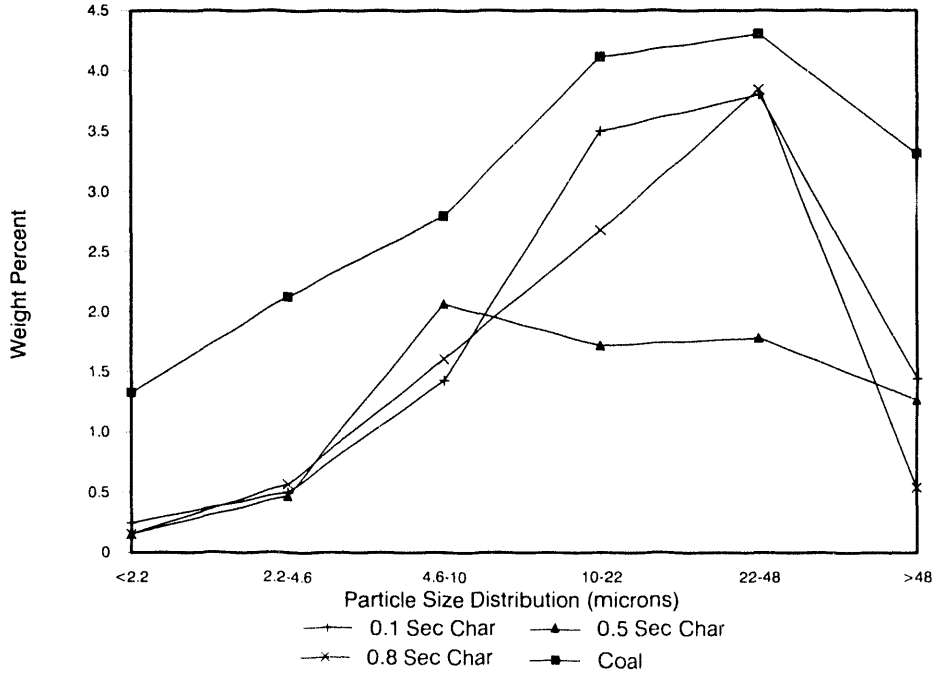

Figure 47. Distribution of quartz in Beulah coal and chars during combustion.

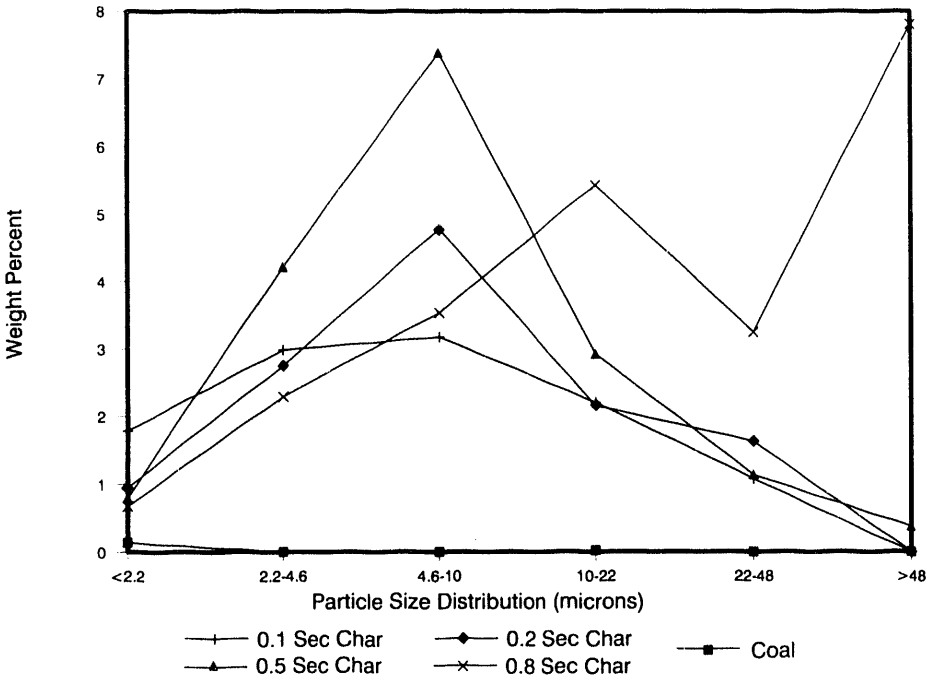

Figure 48. Distribution of Ca-aluminosilicate in Beulah coal and chars during combustion.

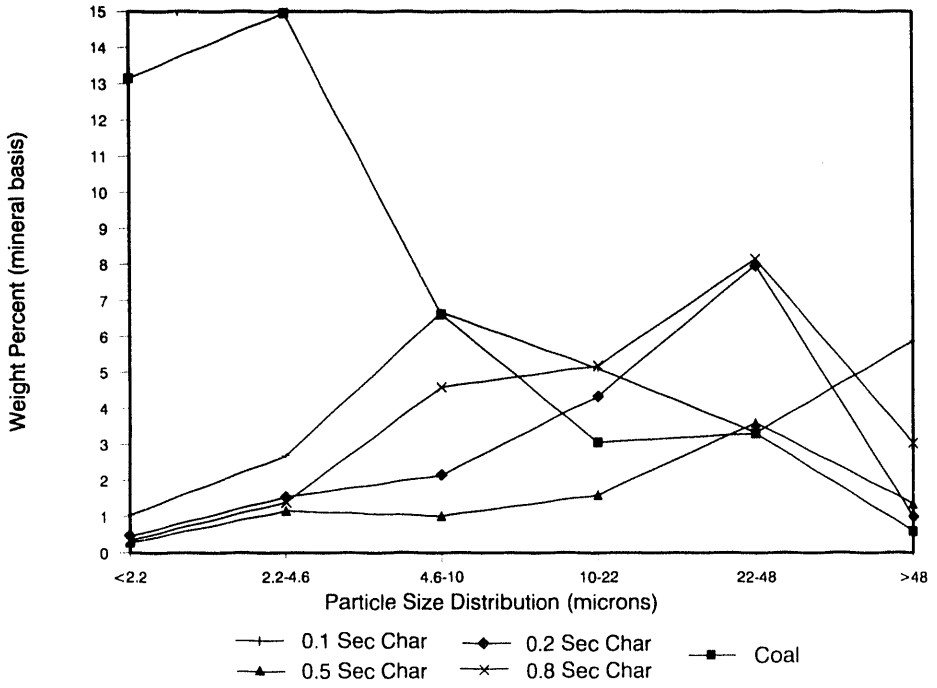

Figure 49. Distribution of aluminosilicate in Beulah coal and chars during combustion.

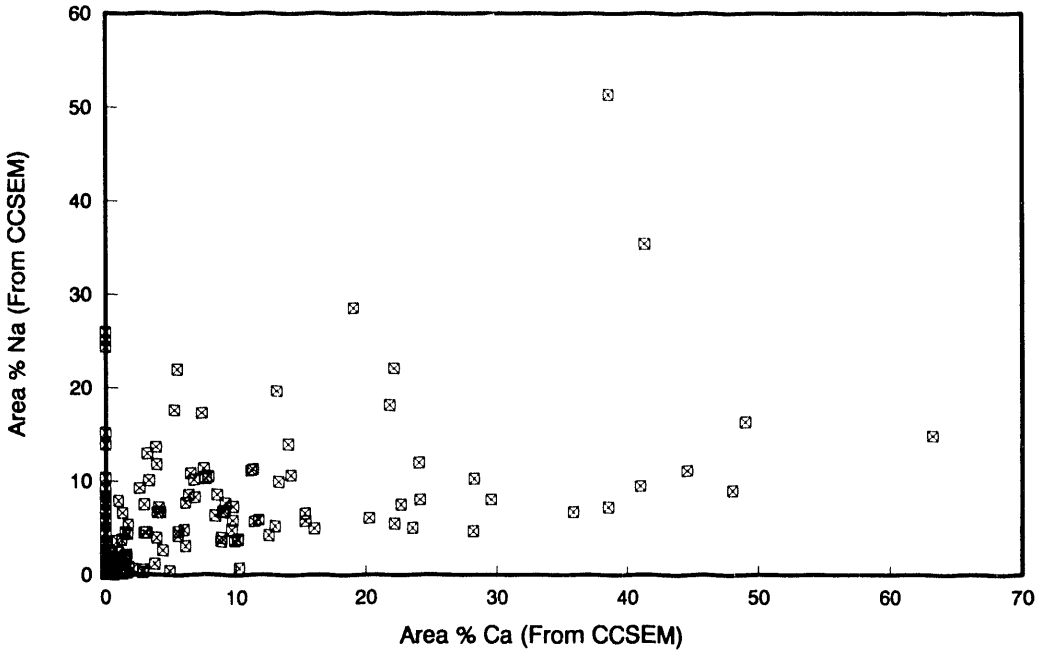

Figure 50. Scatter plot of Na quantity as a function of Ca quantity in Beulah fly ash aluminosilicates.

Pyrite is a major constituent in the Beulah coal, comprising 26% of the coal minerals. Upon combustion, the content of pyrite decreases dramatically as displayed in Figure 51. This would be expected since pyrite readily converts to pyrrhotite and then to forms of iron oxide beginning at temperatures as low as 500°C (25). Indeed iron oxide, which was not present in the coal, was detected by CCSEM in the chars (Figure 52). The sizes of the iron oxide particles were similar to those observed for the pyrite, except there was a slight increase in material noted in the 4.6-10-μm category which may be evidence for fragmentation of pyrite.

3.13.1.2 Upper Freeport

The particle-size distribution for mineral phases in the Upper Freeport chars (Figure 53) shows an initial increase in the number of particles in the smaller size categories. By 0.8 seconds, however, larger quantities of phases are found in the >11.0-μm fraction than in the coal. Weight percent distributions present evidence of coalescence of inorganic ash particles with quantities of minerals being reduced in the <10-μm range and increased in the 22-46-μm range with time (Figure 54). These trends may indicate that, initially, fragmentation of mineral grains may be occurring with subsequent coalescence of ash particles as time in the hot zone progresses.

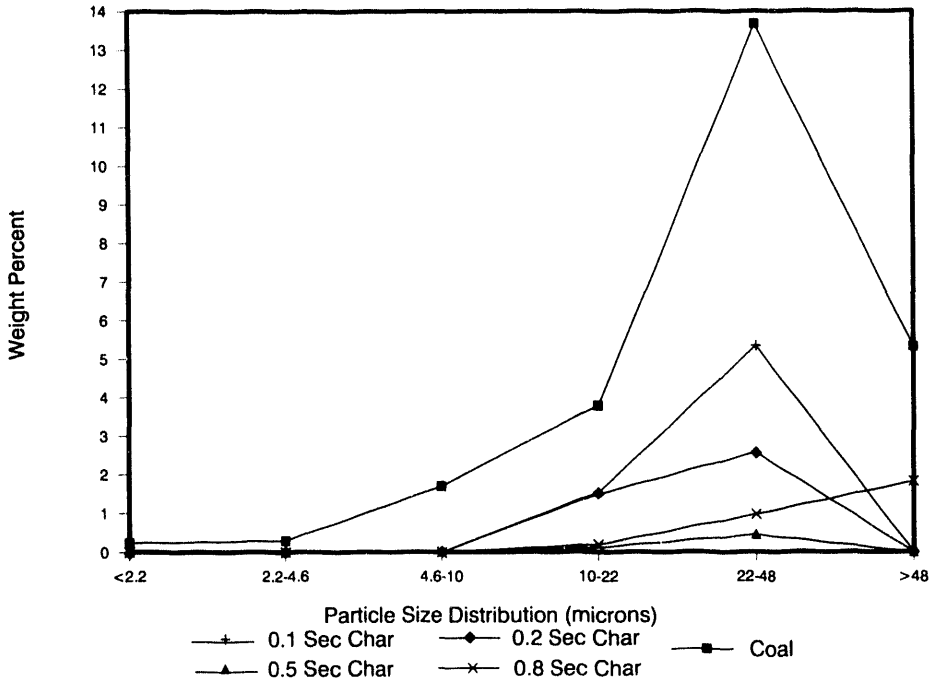

Figure 51. Distribution of pyrite in Beulah coal and chars during combustion.

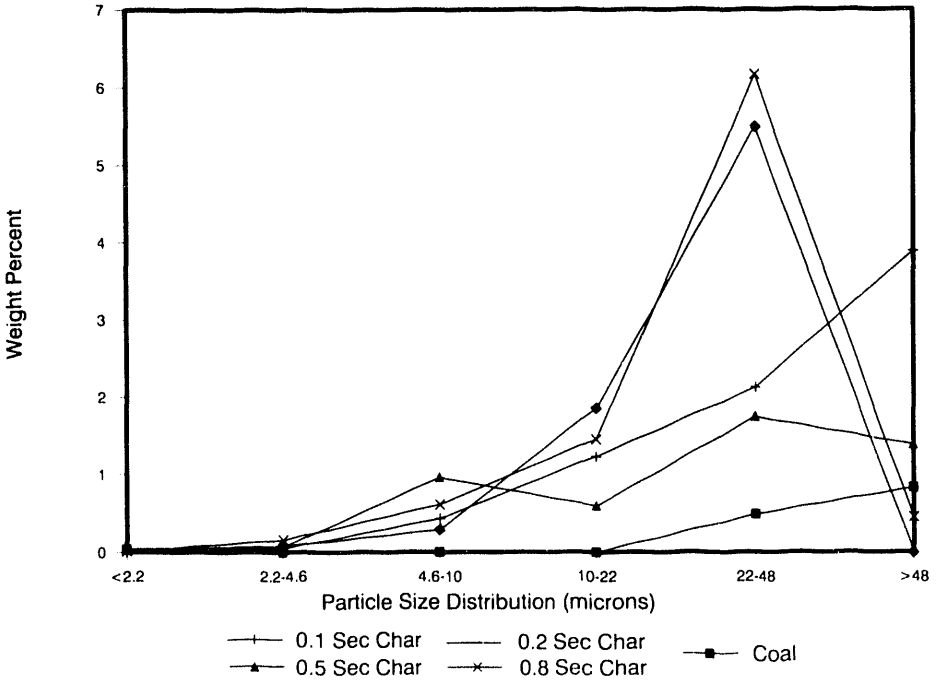

Figure 52. Distribution of iron oxide in Beulah coal and chars during combustion.

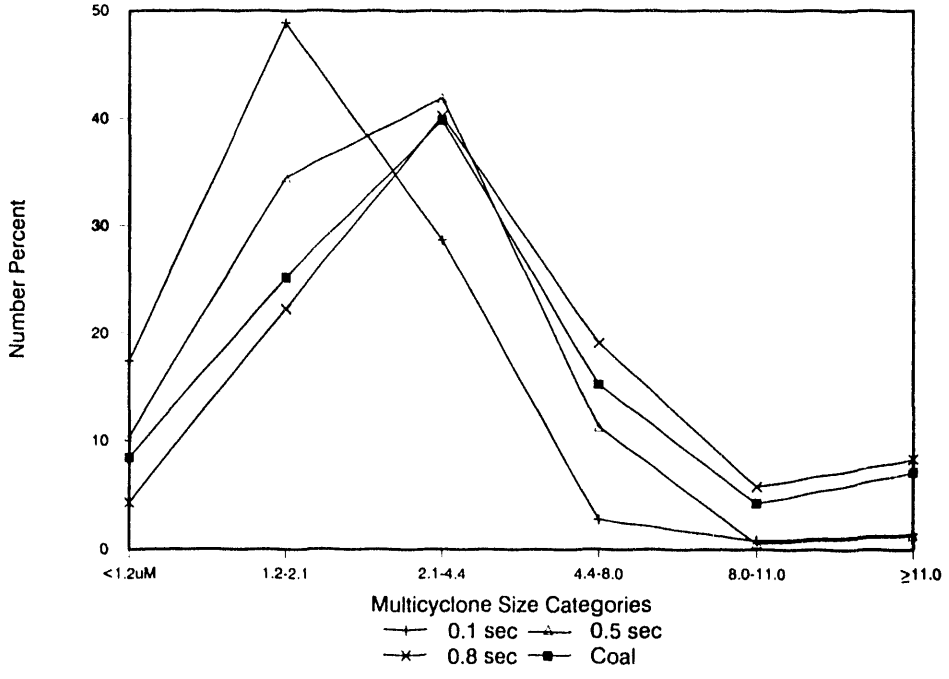

Figure 53. Cross-section particle-size distribution of Upper Freeport coal and char phases during combustion.

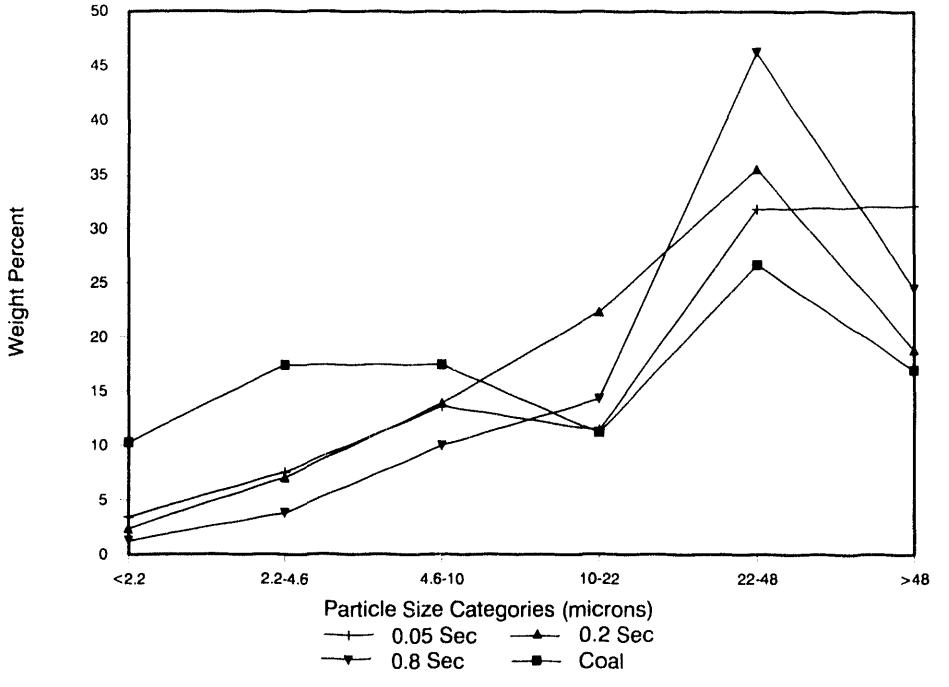

Figure 54. Cross-section particle-size distribution of Upper Freeport coal and char phases.

Iron aluminosilicates have often been associated with wall slagging in boilers that fire bituminous coals such as the Upper Freeport; therefore, the formation of this phase is of prime interest. Figure 55 indicates that iron aluminosilicate particles were produced in the char mostly in the 22-46-μm size range. Some coalescence of existing iron aluminosilicate minerals in the coal may have occurred also. Sources of Fe and aluminosilicate material for the additional iron aluminosilicate phases produced were probably pyrite or iron oxide for Fe and kaolinite or illite for the aluminosilicate. Iron is also present in the illite, reaching levels of 5% of the illite chemical composition.

Illite was originally bimodally distributed in the Upper Freeport coal at 2.2-4.6 μm and 22-46 μm, but, upon combustion, the smaller illite grains coalesced forming a unimodal distribution about the median of 22-46 μm (Figure 56). The shift of material from the smaller size ranges appears to correlate or compensate in crude mass balance fashion with the increase at the larger size range.

Pyrite decomposed to iron oxide in much the same manner as with the Beulah, except that by 0.8 seconds the pyrite composition was either completely destroyed or unrecognized by CCSEM (Figures 57 and 58). The iron oxide quantities produced (Figure 58) do not account for all the released iron from the pyrite. This may indicate that some of the released iron oxide has, by this time, reacted with aluminosilicate to form iron aluminosilicate.

3.14 Summary and Conclusions

Particle-size distributions of discrete mineral or amorphous phases in intermediates produced in the drop-tube furnace (DTF) for two coals were examined. Time-resolved PSD's of phases show that Beulah and Upper Freeport phases coalesce with time. The Upper Freeport shows an initial increase in the amount of particles in the lower size ranges due to fragmentation of minerals or the formation of smaller inorganic ash droplets from submicron minerals or inorganics. The transformation of selected inorganic components through time was also noted. Sodium and calcium organically associated in the Beulah react readily with smaller-sized kaolinitic clays and, to a much lesser degree, with quartz. Pyrite appears to undergo fragmentation during combustion in the Beulah and Upper Freeport, with a resulting increase in iron oxide. The effect of fragmentation of Beulah pyrite on the overall PSD is less pronounced than what has been observed elsewhere (25, 26, 27).

Interpretation of Fly Ash Particle-Size Evolution for San Miguel and Kentucky #9. Volumes of individual fly ash particles were calculated from particle diameters measured using CCSEM. Kentucky #9 and San Miguel coals were combusted at 1500°C and the fly ash particle size analyzed by CCSEM. The coal was sized with Malvern analysis, and the minerals in the coal and the fly ash were sized with CCSEM.

Figure 59 shows the Kentucky #9 particle-size distributions for DTF fly ash, coal minerals, and theoretical fly ash. The theoretical fly ash particle-size distribution assumes that all of the ash in each coal particle coalesces to form one spherical fly ash particle. The minerals are assumed to